

See discussions, stats, and author profiles for this publication at: <https://www.researchgate.net/publication/336985483>

Improving weather radar precipitation maps: A fuzzy logic approach

Article in *Atmospheric Research* · October 2019

DOI: 10.1016/j.atmosres.2019.104710

CITATION

1

READS

190

4 authors, including:



Micha Silver

Ben-Gurion University of the Negev

21 PUBLICATIONS 59 CITATIONS

[SEE PROFILE](#)



Tal Svoray

Ben-Gurion University of the Negev

108 PUBLICATIONS 1,779 CITATIONS

[SEE PROFILE](#)



Arnon Karnieli

Ben-Gurion University of the Negev

281 PUBLICATIONS 10,399 CITATIONS

[SEE PROFILE](#)

Some of the authors of this publication are also working on these related projects:



ECOPOTENTIAL [View project](#)



Acacia trees - population genetics [View project](#)

Improving Weather Radar Precipitation Maps: A Fuzzy Logic Approach

Micha Silver^b, Tal Svoray^a, Arnon Karnieli^b, Erick Fredj^{c,*}

^a*Dept. of Geography and Environmental Development and Dept. of Psychology, Ben Gurion University*

^b*Remote Sensing Lab, Sde Boker Campus, Ben Gurion University*

^c*Jerusalem College of Technology, Jerusalem*

Abstract

Weather radar can provide spatially explicit precipitation grids. However interference, ground clutter and various causes of attenuation introduce uncertainty into the result. Typically, rain gauge observations, recognized as a precise measure of precipitation at point locations, are used to adjust weather radar grids to obtain more accurate precipitation maps. This adjustment involves one or more of various geostatistic techniques. Yet, since gauges are sparsely located, a geostatistic approach is sometimes limited or even not applicable.

This work adopts an alternative to radar adjustment by merging location-based variables with rain grids from weather radar. Recognizing that location-based variables: elevation, slope, aspect and distance from the coast all affect precipitation, these are applied to the original weather radar grid to produce an altered precipitation distribution.

The merging procedure presented here uses fuzzy logic, whereby all variables, as well as the original radar are assigned probabilities known as membership functions (MF), then a joint membership function (JMF) combines all MFs in the fuzzy set, each multiplied by its weight, to create a precipitation probability grid. This JMF probability grid is validated with gauge observation data. We show up to 30% higher correlation coefficients between gauges and the JMF grid than between gauges and the original radar. The improved correlation results from the flexibility of fuzzy logic in transforming location-based variables to probabilities.

Keywords: fuzzy logic, precipitation, gauges, weather radar, location-based

*Corresponding author

Email addresses: silverm@post.bgu.ac.il (Micha Silver), tsvoray@bgu.ac.il (Tal Svoray), karnieli@bgu.ac.il (Arnon Karnieli), fredj@jct.ac.il (Erick Fredj)

1. Introduction

1.1. Background

Estimating spatially distributed precipitation grids is a prerequisite to flood management and flood forecasting (Merz et al. (2014)). Hydrological models need basin-scale, spatially explicit precipitation data, among other inputs, to construct accurate flood forecasts (Todini et al. (2005)) for surface runoff management. Rain radar can produce such spatial precipitation distributions, however the challenges in calibrating and correcting for the various sources of error (detailed in Villarini et al. (2008)) create spatial and temporal uncertainty in the precipitation distribution (Cecinati et al. (2017), Krajewski and Smith (2002)). Nevertheless, the underlying motivation for research in improving precipitation maps rests in the needs of hydrological modeling and flood forecasting.

Since weather radar became an accepted source of spatially distributed rainfall (Krajewski and Smith (2002), Morin et al. (2003)), extensive research has examined adjustment procedures to merge rain gauge observations with weather radar. Gauge data are accepted as reference observations (see for example Colli et al. (2013)), but represent point locations. Such point data can adjust weather radar grids through several geostatistic methods, reviewed and evaluated by Goovaerts (2000), Berndt et al. (2014) and McKee and Binns (2016). Kriging based methods have been examined by Kebaili Bargaoui and Chebbi (2009), Adhikary et al. (2017), and Ly et al. (2013). A comparison of various kriging methods where elevation was the secondary variable was done by Carrera-Hernández and Gaskin (2007). Another unique algorithm known as Conditional Merging, developed and evaluated by Sinclair and Pegram (2005), applies multiple kriging steps to achieve successful adjustment (Kim et al. (2007)) of weather radar grids.

However the density of gauge observations, required for successful adjustment and described by Otieno et al. (2014), is often lacking. The limitation of gauge density is especially severe in third world countries (Dieulin et al. (2019)) but also affects precipitation modeling in European countries, such as Paulat et al. (2008). In addition, globally the number of accurate and automated gauges is dropping (Kidd et al. (2017)), further challenging the variety of geospatial adjustment techniques above. On that background, this current work presents a method to improve radar precipitation grids independently of any gauge network, using location-based variables instead.

1.2. Fuzzy logic models

Since the seminal works on fuzzy systems (Zadeh (1965) and Zadeh (1975)) that modeling approach has been thoroughly debated (see i.e. Zadeh (2008) for a review and response to criticism). However over the past decades, fuzzy logic and fuzzy systems have been widely adopted in the scientific community (i.e. Guiffrida and Nagi (1998) and chapter 13 of Zimmermann (2013)). Fuzzy systems consider a range of independent variables to predict some outcome. However, unlike other models, the input variables do

39 not have exact values, rather they present probabilities of the influence of each variable
40 on the final outcome. These probabilities are combined in a joint membership function
41 to predict some explicit, clear cut output.

42 Fuzzy logic models were applied to remote sensing as early as [Foody \(1996\)](#). [Foody](#)
43 [\(2002\)](#) evaluated uncertainty in land-cover classification models and showed that a fuzzy
44 logic model reduces that uncertainty. Accuracy of landcover classification from historical
45 aerial photography was validated using fuzzy sets by [Okeke and Karnieli \(2006\)](#). A soil
46 erosion model based on fuzzy logic equations was developed by [Cohen et al. \(2008\)](#) and
47 shown to improve runoff and erosion predictions in both small and large scale catchments
48 compared to another conventional model. Vegetation patches in an arid environment were
49 modeled using fuzzy logic by [Svoray et al. \(2007\)](#). Multiple soil and climate variables
50 were applied in a fuzzy set model by [Svoray et al. \(2008\)](#) to model biomass production. In
51 more recent research [Comber et al. \(2012\)](#) performed Geographically Weighted Regression
52 (GWR) on two land-cover data sets, one derived from classic remote sensing classification,
53 and the other from a fuzzy logic method. They found that applying GWR to the two
54 data sets can reduce uncertainty in a final land-cover product.

55 Among the early applications of fuzzy logic to weather modeling was [Hundecha et al.](#)
56 [\(2001\)](#) where the rainfall-runoff relation was evaluated. [Berenguer et al. \(2006\)](#) exam-
57 ined the possibility of applying fuzzy logic to identify anomalous propagation in radar
58 reflectance. An interesting effort by [Yang et al. \(2013\)](#) and an earlier conference report
59 by [Wang et al. \(2012\)](#) applied fuzzy logic to weather radar to discriminate convective
60 from stratiform storm types. Later both [Krause \(2016\)](#) and [Dufton and Collier \(2015\)](#) ex-
61 panded on that work and presented methods for discriminating several non-hydrological
62 echos in Doppler weather radar using fuzzy logic. [Asklany et al. \(2011\)](#) used a fuzzy
63 system to predict rainfall events, where the inputs consisted of climate variables and the
64 fuzzy rule base was composed of a series of if-then conditions. Additionally, [Giap \(2014\)](#)
65 presented a fuzzy based method to identify faulty rain gauges. [Agboola et al. \(2015\)](#)
66 developed a fuzzy logic based model to predict precipitation based on a collection of
67 climate variables. Also in [Men et al. \(2017\)](#) a fuzzy clustering algorithm was developed
68 to forecast rainfall. Finally, flood risk was modeled by [Wijitkosum and Sriburi \(2019\)](#)
69 using a combined fuzzy logic and an analytical hierarchy process. They used a collection
70 of meteorological variables, soil characteristics and anthropogenic factors.

71 The fuzzy set approach allows describing the independent variables as probabilities, or
72 membership functions (MF), rather than rigid variables as in regular regression models.
73 Advanced machine learning regression algorithms also create a best-fit model from a
74 set of rigid variables. Interestingly, the combined fuzzy-neural network approach ([Jang](#)
75 [\(1993\)](#)) has seen renewed interest (for example [Besalatpour et al. \(2012\)](#), [Hong et al.](#)
76 [\(2018\)](#)). The fuzzy set approach incorporates flexibility in mapping the variables to a
77 probability function that cannot be attained in a regression approach. Yet the fuzzy
78 model result, as expressed in the joint membership function (JMF) produces a definitive,

79 clear cut output by combining the influences of all independent variable MF probabilities.

80 1.3. Independent variables

81 Previous research applying fuzzy logic to determine precipitation (mentioned above
82 in Section 1.2) choose meteorological variables such as temperature, humidity, or snow
83 depth. The current work analyzes location-based variables: elevation, slope, aspect, and
84 distance from the coast, as well as rain radar precipitation grids.

85 The correlation between rainfall and elevation, probably due to orographic forcing, has
86 been well documented (for example: [Goovaerts \(2000\)](#), [Daly et al. \(1992\)](#) and [Carrera-
87 Hernández and Gaskin \(2007\)](#)). [Guan et al. \(2005\)](#), working in a mountain region of New
88 Mexico, applied a window surrounding rain gauges, and found high correlation between
89 the gauge observations and elevation within the window. [Lassegues \(2018\)](#) researched
90 aggregated rainfall and elevation in the western Alps with a relatively high density of
91 gauges and applying geostatistic spatial analyses. Another recent research paper by [Tang
92 et al. \(2018\)](#) reported correlation between precipitation data from the Tropical Rainfall
93 Measuring Mission (TRMM) and elevation in the Tibetan plateau. Slope as a variable
94 was examined by [Sanchez-Moreno et al. \(2014\)](#), along with elevation using 30 years of
95 monthly aggregated rainfall data in Cape Verde. They found that, in some seasons, slope
96 was better correlated to precipitation than elevation.

97 Research on precipitation and proximity to the coastline has consistently found higher
98 rainfall levels near the coast ([Hayward and Clarke \(1996\)](#)). Some of this work focuses on
99 the difference between forested and non-forested regions, for example [Makarieva et al.
100 \(2009\)](#). Working with a global database of gridded monthly average precipitation, they
101 report an exponential drop in precipitation level with distance from the coast in non-
102 forested regions. In a different climatic region, [Daniels et al. \(2014\)](#) analyzed changes
103 in precipitation in the Netherlands over a 60 year period. Their statistical analysis took
104 into account variables such as soil type and slight changes in elevation, as well distance
105 from the coast. They reported that the highest precipitation levels were in the first two
106 coastal zones, up to 100 km. from the coastline. [Ogino et al. \(2016\)](#) examined global
107 data from TRMM and showed sharp drops in elevation within 300 km from coastlines in
108 tropical regions.

109 Weather radar has been used for decades to produce rainfall grids. Indeed, sev-
110 eral national weather services distribute gauge adjusted radar images continuously (i.e.
111 the German Deutcher Wetterdienst (DWD) ([https://www.dwd.de/EN/ourservices/
113 radar_products/radar_products.html](https://www.dwd.de/EN/ourservices/
112 radar_products/radar_products.html)) and the Royal Netherlands Meteorological Ser-
114 vice (<https://data.knmi.nl/datasets>). Radar derived rain rates are affected by sev-
115 eral sources of uncertainty ([Krajewski and Smith \(2002\)](#), [Sebastianelli et al. \(2013\)](#)), yet
116 these data cover the region with a continuous grid of relatively high resolution ([Morin
117 et al. \(2003\)](#)). Although not a location-based variable, weather radar provides the model
with the crucial base precipitation grid, with which the other four variables are merged.

118 Aspect, defined as the compass direction of slope faces, adds to the model a compo-
119 nent of synoptic conditions. When a storm proceeds across the study area in some dis-
120 tinct direction, then slopes facing the storm will experience higher rainfall (Reid (1973)).
121 Working in the Tibetan plateau, Tang et al. (2018) compared satellite-borne rain de-
122 tectors (Global Precipitation Measurement (GPM) and TRMM) to gauge observations,
123 and also found correlation between precipitation and wind-facing slopes. In addition
124 Guan et al. (2005) applied multivariate regression to gauge data, using terrain variables,
125 including aspect. They reported the highest correlation to precipitation when combining
126 elevation, aspect and atmospheric moisture.

127 At smaller scales, both Sternberg and Shoshany (2001) and Kadmon and Danin (1999)
128 investigated tree and shrub biomass in a Mediterranean climate as a function of aspect,
129 and both found that storm facing slopes had higher water availability, and thus higher
130 biomass. Work by Arazi et al. (1997) and Sharon and Arazi (1997) analyzed the effects
131 of wind on precipitation rates in small catchments. Similarly Sevruk and Nevenic (1998)
132 researched the wind-induced effects of rainfall measurements, comparing the windward
133 versus leeward spatial distribution of precipitation. However their work focused on local,
134 micro-topography.

135 A long term classification of synoptic events in the eastern Mediterranean, published
136 in Alpert et al. (2004), was adopted in this current work to find the proportion of storm
137 directions for each month during the study period. Using their dataset, we determined
138 for each month what percent of storms moved into the region from each compass direc-
139 tion. Then the aspect grid was used to determine storm facing slopes at the pixel level.
140 Thus, inclusion of both slope and aspect as variables in the current research added novel
141 components to the model.

142 1.4. Temporal aggregation

143 The model and validation presented in this work refer to monthly aggregated rainfall.
144 The limitations of correlating precipitation measurements from different sources at short
145 time intervals has been discussed by Kirstetter et al. (2010), Marra and Morin (2018)
146 and others. These limitations result from several spatial and temporal discrepancies
147 between gauges and radar: gauges are point measurements while radar is represented
148 on a grid; wind drift and the time gap between rain droplets in the clouds and rainfall
149 on the ground cause time shifts; and the timing of radar sweeps and gauge aggregation
150 intervals are often different. Marra and Morin (2018) examined temporal auto-correlation
151 from one minute X-band weather radar, and showed high correlations only when data was
152 aggregated to extended time intervals. Similarly Kirstetter et al. (2010) prepared analyses
153 of residuals between radar and gauge observations and presented increased values for R^2 ,
154 mean relative error and Nash Sutcliffe coefficients as the time interval increased. Research
155 by Sideris et al. (2014) produced accurate adjusted rainfall grids using co-kriging of
156 several time steps from earlier radar images. Yet even in that research the problems

157 associated with correlation of rainfall data at small temporal resolution were raised. In
158 the current work, both weather radar grids and gauge observations were aggregated over
159 a month to insure that temporal resolution effects were avoided.

160 *1.5. Objectives*

161 This current work departs from the usual geostatistic approach described above. A
162 spatial distribution of precipitation from weather radar is produced by applying fuzzy
163 logic to a set of five variables: the weather radar itself, elevation, slope, aspect, and
164 distance from coast.

165 The objectives of this research include:

- 166 • Use fuzzy logic to improve weather radar precipitation maps;
- 167 • Apply location-based variables to the newly developed methodology;
- 168 • Validate the precipitation maps with gauge observations at two time intervals:
169 monthly and daily (individual storm events) aggregations;
- 170 • Highlight the advantage of the fuzzy approach in the context of weather radar
171 precipitation.

172 **2. Methodology**

173 This section details the procedures to download required data, create probability
174 raster layers for the variables described in Section 1.3 above, and prepare and analyze
175 the final JMF. The GRASS-GIS ([Neteler et al. \(2012\)](#)) commands and additional python
176 scripts will be made available on request.

177 *2.1. Study area and data acquisition*

178 This work focuses on two climatic zones in the eastern Mediterranean region: an arid
179 zone in southern Israel (Köppen-Geiger classification (as in [Kottek et al. \(2006\)](#)) BWh
180 and BSh), and a Mediterranean climate in the north (Köppen-Geiger CSa). The northern
181 study area experiences annual rainfall between 400-900 mm/yr. The southern region, on
182 the other hand, is semi-arid to arid, receiving only 50-250 mm/yr. Weather radar data
183 were available from two C-band (5.6 GHz.) radar stations, near Mitzpeh Ramon in the
184 south, and Safed in the north (see Figure 1), covering a study period of four winter (wet
185 season) months: January, October, November and December, 2018 as well as January,
186 2019. Raw data from these radar stations were pre-processed (using the *wradlib* library,
187 [Heistermann et al. \(2013\)](#)) as follows:

- 188 1. Only three lower elevation angles were considered: -0.5° , 0.9° and 2.3° ;
- 189 2. Three corrections were applied to each individual radar file: Path Integrated At-
190 tenuation, Beam Blockage, Ground Clutter removal;

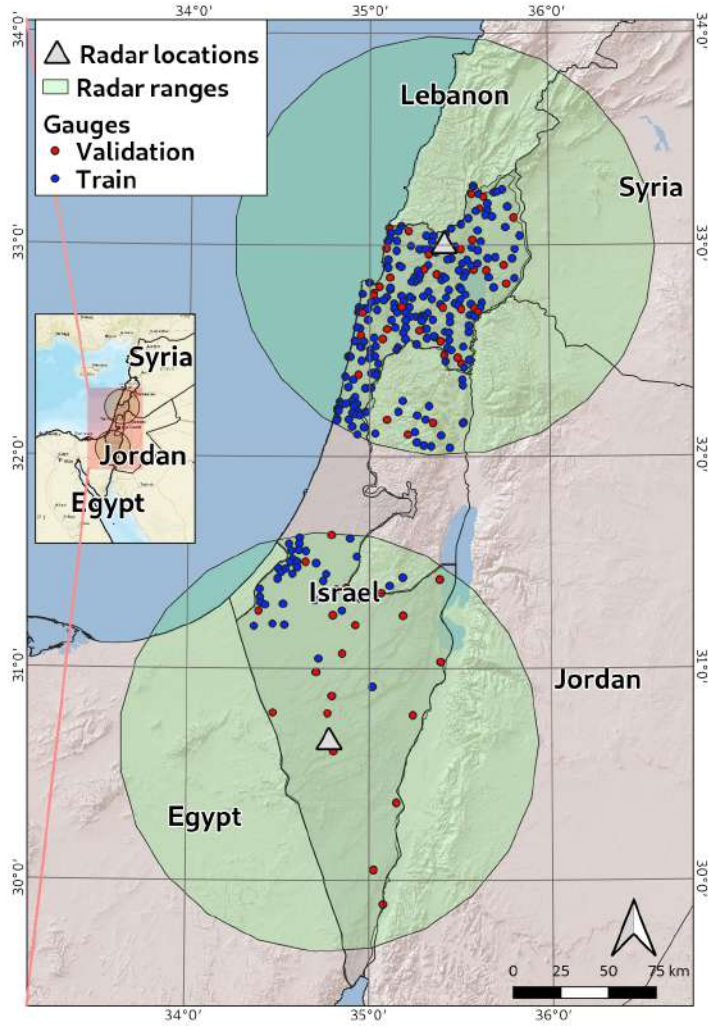


Figure 1: Study area, radar ranges and gauge locations. The northern radar covers a region with Mediterranean climate, and the southern radar covers an arid region. Rain gauge locations are categorized as training and validation (Section 2.1)

3. dBZ (from raw radar data) was converted to rainfall depth using the standard Z-R power law, Equation 1:

$$R = \left(\frac{Z}{a} \right)^{(1/b)} \quad (1)$$

191 where $a=316$ and $b=1.5$ following arid region power law parameters in [Morin and Gabella \(2007\)](#);
 192

- 193 4. The radar stations changed scan mode (sweep speed, and elevation angles) occa-
 194 sionally. The three scan modes were treated separately, and data was aggregated
 195 only after applying corrections;

196 5. Data was aggregated by hour, day, and month;

- 197 6. A full seasonal aggregation was also prepared and used to extract range degrada-
 198 tion parameters, using the approach in [Morin and Gabella \(2007\)](#) for arid regions.
 199 Linear regression slope and intercept were determined from the radar/gauge ratio
 200 compared to distance of gauges from the radar. These were then applied to each

- 201 monthly aggregation to correct for range degradation.
- 202 7. A Mean Field Bias adjustment factor was determined as the quotient of mean
203 range-corrected radar values and mean gauge values. This multiplicative factor
204 was then applied to each monthly aggregation;
- 205 8. The original Polar coordinate system was projected and resampled to a Cartesian,
206 georeferenced coordinate system of 1 km. resolution.

207 Gauge data were obtained from the Israel Meteorological Service¹ (IMS) at both
208 monthly and daily accumulation intervals for the months of the study period. A total of
209 61 automatic (online) gauges contained data for these time periods: 24 in the southern
210 and 37 in the northern study areas. Also daily aggregations were acquired for specific
211 storm events, October 25, 2018, December 7, 2018 and January 16, 2019. Metadata,
212 also acquired from the IMS website, contained longitude/latitude for each gauge. The
213 aggregated monthly precipitation, once joined to the gauge metadata, created point layers
214 of monthly aggregated observations used in this work for validation (Section 2.4).

215 The IMS also maintain a larger network of gauges that are manually checked each
216 day. From personal communication, the IMS consider both sets of gauges equally reliable
217 with data collection intervals of 10 minutes in both cases. This second set of manual
218 gauges, 266 of which fell in the two study areas, was used to determine radar correction
219 parameters as described above. Both sets of gauges are well distributed throughout the
220 country (as displayed on the map in Figure 1), thus by splitting the full set of IMS gauges
221 according to gauge type, automatic or manual, a larger set of data was used for tuning
222 the model and radar correction, and a smaller, independent set for validation.

223 An elevation grid covering the study area was acquired from the Shuttle Radar Terrain
224 Mission (SRTM) program² at 3 arc seconds (about 90 meters) resolution. In addition
225 to serving as elevation data for the study area, this layer was also processed to produce
226 slope and aspect grids, which became components of the fuzzy set. These elevation, slope
227 and aspect grids were all downscaled to 1 km. resolution to match the Cartesian grid of
228 the radar data.

229 *2.2. Membership functions and probabilities*

230 This work focused on location-based variables. Five variables were considered which
231 affect precipitation:

- 232 1. Elevation;
- 233 2. Distance from the coastline;
- 234 3. Slope;
- 235 4. Aspect;
- 236 5. Rainfall from weather radar.

¹from: <https://ims.data.gov.il/> , in hebrew

²from <ftp://edcsgs9.cr.usgs.gov/pub/data/srtm/version1>

237 Having chosen the influencing variables (Section 1.3), a MF was assigned to each,
 238 thereby constructing the fuzzy set. MFs are represented by probability curves that
 239 span the range of possible values for each variable. The MF maps variable values to
 240 probabilities (with values from 0 to 1.0). Figure 2 shows the MF probability curves for
 241 each variable. Three of the variables are static throughout the study period: elevation,
 242 slope and distance from coast. Each was represented by an “S” shaped curve (Equation
 243 2) given by the exponent of a *sine* curve with two turning points p_0 and p_1 (following
 244 Klir and Yuan (1995), chapter 1 and implemented as in Jasiewicz (2011)).

$$MF = \begin{cases} 0 & v_x \leq p_0 \\ \sin(v_x \cdot \frac{\pi}{2})^2 & v_x > p_0 \text{ and } v_x \leq p_1 \\ 1 & v_x > p_1 \end{cases} \quad (2)$$

245 where v_x is the vector of possible variable values.

Table 1: Turning points for each curve

Variable	Min. value	p_0	p_1	Max. value
Elevation	-400	10	330	1000
Dist. from coast	0	50	100	220
Slope	0°	4°	20°	34°
Aspect	(rectangular function, described in the text)			
Radar	R_{\min}	$0.01 \cdot (R_{\max} - R_{\min})$	$0.9 \cdot (R_{\max} - R_{\min})$	$R_{\max} - R_{\min}$

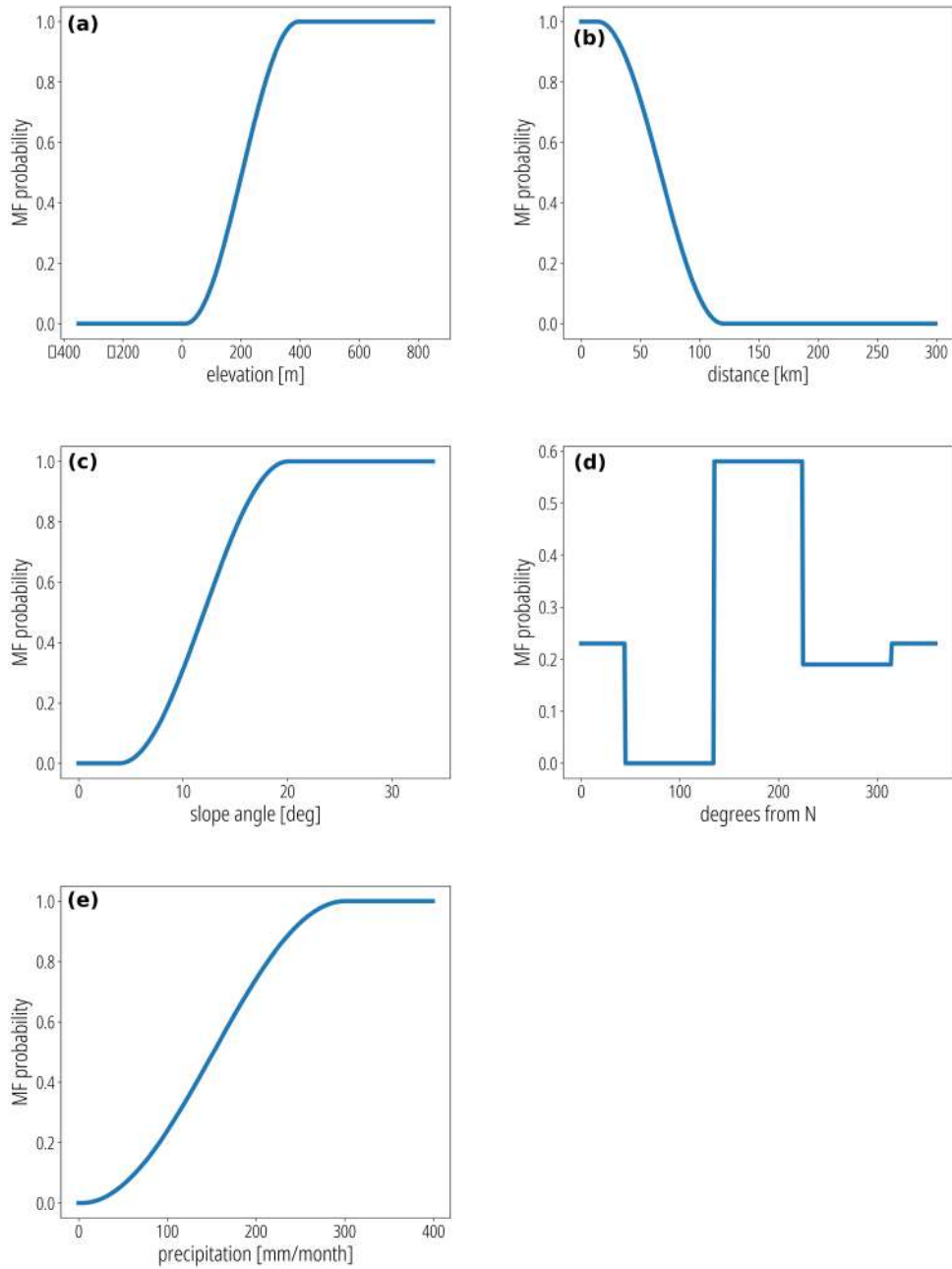


Figure 2: Static and monthly varying membership function curves. (a) Elevation, (b) Distance from coast, (c) Slope, (d) Aspect, (e) Radar

246 The turning points, listed in Table 1, were chosen as a percent of the full range of
247 each variable. Thus the elevation MF varies from 400 m. below sea level (the Dead Sea
248 area) to 1000 m., the peak elevations in the northern study area. The lower turning
249 point was chosen at 10 m., just above sea level, and the second at 330 m., a third of
250 the maximum elevation. Thus all low elevations got precipitation probabilities near to
251 zero. The probability then rose quickly, reaching 1.0 at elevation 400 m. The coastal
252 plain in the study areas includes elevation to over 200 m., while 300 m. and above are
253 mountainous. Thus the chosen turning points set low to moderate probability for the
254 coastal plain and high probability in the mountain regions. This choice reflected past
255 research (cited in Section 1.3) which showed the effects of elevation on precipitation.

256 Similarly, the slope MF varied from 0° to a maximum of 34° slope angles. All flat
257 areas, up to 4° were designated zero probability, then for moderate slopes of 4° to 10°
258 probability increased rapidly, reaching 1.0 at slope above 20° .

259 The distance from coast MF curve behaves inversely, with the high turning point at
260 50 km. and low turning point at 100 km. In this way, the coastal areas gained high
261 probability values, whereas far to the south, the arid region dropped to zero probability.
262 Research on the correlation between precipitation and distance from the coast (sources
263 cited in Section 1.3) indicated that inland precipitation is affected by the sea up to a few
264 hundred kilometers from the coast, justifying the distances chosen above.

265 The other two MF's varied from month to month. The radar MF reflects the aggre-
266 gated monthly precipitation from radar data, thus each month had a different probabili-
267 ty MF curve. However all monthly curves were prepared in the same way. Minimum
268 and maximum precipitation values (R_{min} and R_{max}) were extracted from the monthly
269 weather radar aggregation. The maximum was determined after removing outlier values,
270 where outliers were defined as values above the 98th percentile. From visual inspection
271 of the radar images, these outlier pixels were assumed to result from non-meteorological,
272 high reflectance ground clutter that persisted even after ground clutter removal. Then
273 turning points were set at $p_1 = 0.9 \cdot (R_{max} - R_{min})$ and $p_0 = 0.01 \cdot (R_{max} - R_{min})$ and
274 the "S" curve equation 3 was then applied.

275 The resulting radar MF probability curve transformed low radar precipitation to
276 almost zero probability, then the curve rose slowly; only the pixels with heaviest monthly
277 aggregated rainfall were transformed to probability of 1.0. Justification for this radar MF
278 originates from the various sources of uncertainty in weather radar that are not dependent
279 on rainfall intensity. Villarini and Krajewski (2010) as well as Chumchean et al. (2003)
280 and others reviewed sources of uncertainty in deriving rainfall from radar reflectance.
281 Errors associated with beam blockage, polar-Cartesian conversion and calibration of the
282 radar are independent of the rain intensity. Also wet radome effect and to some extent
283 vertical profile of reflectivity do not increase in heavier storms. Thus their relative effect
284 is greater in low intensity rain events. Overall the weather radar signal to noise ratio is
285 low (i.e. high noise level) when rain intensity is low. At high rain intensity, the above

286 sources of error are, to some extent, overcome by the strength of the signal received by
 287 the radar. Therefore, the radar MF was chosen to mirror this uncertainty by assigning
 288 very low probability to low rain intensity, and increasing the probability to 1.0 as the
 289 rain intensity grows towards the monthly maximum.

290 The aspect MF also varies by month, but was handled differently. Rather than an
 291 “S” curve, probability values were determined for each of the four compass directions,
 292 resulting in a rectangular probability function. The probability for each direction was
 293 derived from the proportion of the synoptic classes (see Section 1.3 and Alpert et al.
 294 (2004)) in a particular month. Referring to panel (d) in Figure 2, which represents
 295 January, 58% of the synoptic events during that month were classified Red Sea Trough
 296 (based on data from personal communication and Alpert et al. (2004)), which moves
 297 northward. So all south facing pixels, from 135° to 225° were assigned a probability of
 298 0.58. Approximately 23% of the synoptic events during January were classified as normal
 299 Cyprus Low fronts moving eastward. So west facing aspect angles of 225° to 315° got a
 300 probability of 0.23. In this fashion rectangular MF curves for aspect were prepared for
 301 each month.

302 2.3. Joint membership function

In fuzzy set theory, MFs are combined using one of several types of joint membership
 functions (JMF): intersection, union, exclusive disjunction, or combinatorial. These types
 are explained in chapter 2 of Zimmermann (2013) and other textbooks on fuzzy sets. An
 intersection JMF finds the minimum of all MF probabilities, while a union JMF finds the
 maximum. Exclusive disjunction returns the probability of one MF less the inverse of
 the other MF. A combinatorial JMF is comprised of the sum of all MFs, each multiplied
 by some weight. The JMF in the current work was constructed using a combination of
 all MFs, by summing the products of each variable probability P_{mf} by its weight, w_{mf}
 as in Equation 3. Choice of this type was dictated by the need to include all of the
 location-based variables in calculating the final precipitation grid.

$$JMF = \sum_{allMF} w_{mf} \cdot P_{mf} \quad (3)$$

303 The vector of weights was determined by performing 100 iterations of a global opti-
 304 mization function (using the basin hopping technique). This function calculated the cor-
 305 relation between gauge observations (using the set of manual gauges only) and the JMF
 306 probability at the gauge locations, and found the weights that minimized $1 - correlation$.
 307 The optimization algorithm ended after cycling through 15-25 steps with no change in
 308 the result. Weights were then normalized such that the sum of the weights equaled 1.0.
 309 The final, optimized weight vectors appear in Table 2.

310 Applying the JMF resulted in monthly precipitation probability grids (values from 0
 311 to 1.0) at the same resolution and extent as the original radar precipitation grids. The

Table 2: Optimized weights

Region	Radar	Elevation	Aspect	Slope	Dist. from coast
South	0.13	0.18	0.05	0.08	0.56
North	0.54	0.09	0.02	0.02	0.33

312 authors recognize that hydro-meteorological models require a high temporal resolution
313 of precipitation grids for flood forecasting applications. Therefore, despite the difficulties
314 producing rain grids over short time intervals, an attempt was made to apply the model
315 to three 24 hour periods, with some success (see Section 3). The specific 24 hour periods
316 were chosen to overlap with heavy storm events: October 25, 2018; December 7, 2018;
317 January 16, 2019 to produce JMF probability grids for these individual storms (refer to
318 Section 1.4)

319 2.4. Validation

320 Using the gauge locations (see Section 2.1), pixel values from both the radar grids
321 and the JMF probability grids were extracted. In both cases the values from four pix-
322 els surrounding the gauge location were averaged to overcome local inconsistencies in
323 the probability grid. This resulted in monthly datasets each with pairs of gauge observa-
324 tions/radar precipitations and gauge observations/JMF probabilities. A linear regression
325 was performed on each of the pairs for each monthly data-set, and for the north and south
326 study areas separately.

327 With the small sample size available ($N = 37$ and $N = 20$ in the north and south
328 study areas respectively) concern arose that the coefficient of determination would not be
329 a reliable test of correlation due to non-normal distribution of residuals or heteroscedastic-
330 ity. Residual plots were examined (see Figure 3), and two tests performed: Shapiro-Wilk
331 to check for normality of residuals, and Breusch-Pagan to check for heteroscedasticity.
332 When either of these tests resulted in a p -value < 0.05 , then that served as evidence
333 to reject the null hypothesis (H_0 assumes normal and homoscedastic), and parametric
334 correlation tests such as Pearson should be avoided. One or the other of these tests did
335 suggest rejecting the null hypothesis, and examination of the residuals and QQ-plots con-
336 firmed the suspicion. Therefore the non-parametric Kendall’s tau test for correlation was
337 chosen instead. Correlation results appear in Table 3 for the monthly aggregations, and
338 Table 4 for individual storm events with 24 hour aggregations. The left column of the
339 Kendall’s tau statistic refers to gauges and the radar grid, and the second column refers
340 to correlation between gauges and the JMF probability grid (both at gauge locations).

341 3. Results

342 Once the fuzzy set framework was constructed and validated, two collections of results
343 were produced: scatter plots and precipitation maps. Both were prepared in pairs, on

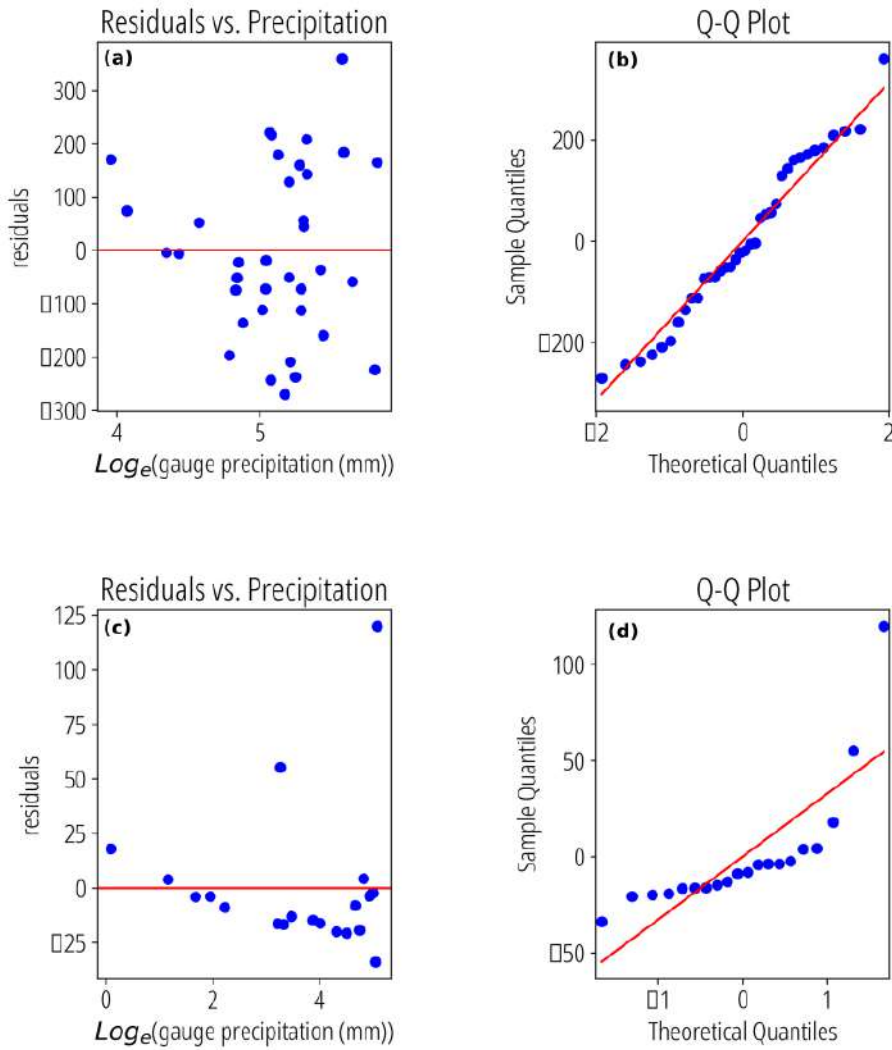


Figure 3: Residuals tests. Residual plots show heteroscedasticity in panels (a) and (c); Q-Q plots, panels (b) and (d) show non-normality of residuals distribution. The graphs (a) and (b) refer to north study area, and panels (c) and (d) refer to south study area.

344 one hand the gauge data compared to radar precipitation and on the other hand gauge
 345 data compared to the JMF derived precipitation.

346 3.1. Scatter plots

347 Initially, gauge precipitation values were plotted against the JMF probability at gauge
 348 locations (averaging four pixels around each gauge location in the JMF grid). Examining
 349 these initial graphs, it became clear that the correlation between gauge data and the JMF
 350 probability was best matched on a log scale. This was expected since four of the MF
 351 probability curves were prepared (see Section 2.2 and equation 3) as functions of \sin^2 ,
 352 suggesting that a best fit linear regression would be obtained using an exponential scale.
 353 Therefore all further correlations compared radar or JMF precipitation grids to \log_e of
 354 the gauge observations.

355 Referring to the scatter plots in Figures 4 to 8 this choice of a log scale for the

356 gauge observations proved to be correct. Each pair of graphs presents the results for one
 357 monthly aggregation, in panels (a) the original radar vs \log_e of gauge observations, and
 358 panels (b) represent the JMF probability vs. \log_e of the gauges. The blue points on all
 359 panel (b) graphs, JMF probability values, show a fairly good fit to the linear regression
 360 line. Scatter plots are presented for two months in the northern region and three months
 361 in the southern region. Results for other months appear in Table 3.

362 3.2. Precipitation maps

Next, the linear regression coefficients, β_1 (the regression rate of change) and β_0 (the regression intercept), were extracted for each month and study region, and were applied to the JMF probability grids to reconstruct the final JMF precipitation grids. These coefficients appear in Table 3. Since the linear regression was applied to \log_e of the gauge values, the equation to reconstruct the JMF predicted precipitation grid was:

$$JMF_{precip} = e^{\left[\frac{JMF_{prob} - \beta_0}{\beta_1} \right]} \quad (4)$$

363 Equation 4 produced JMF predicted precipitation grids for each month and region
 364 in the study. Figures 9 to 12 present the radar based precipitation in panels (a) and the
 365 reconstructed JMF precipitation in panels (b) for two months in both north and south
 366 regions.

367 3.3. Single storm events

368 Also presented, in Table 4, are fuzzy model results from three 24 hour periods: Octo-
 369 ber 25, 2018, December 7, 2018 and January 16, 2019, covering three storm events. The
 370 pair of scatter plots for January 16, 2019 appears in Figure 13 and the accompanying
 371 precipitation maps in Figure 14.

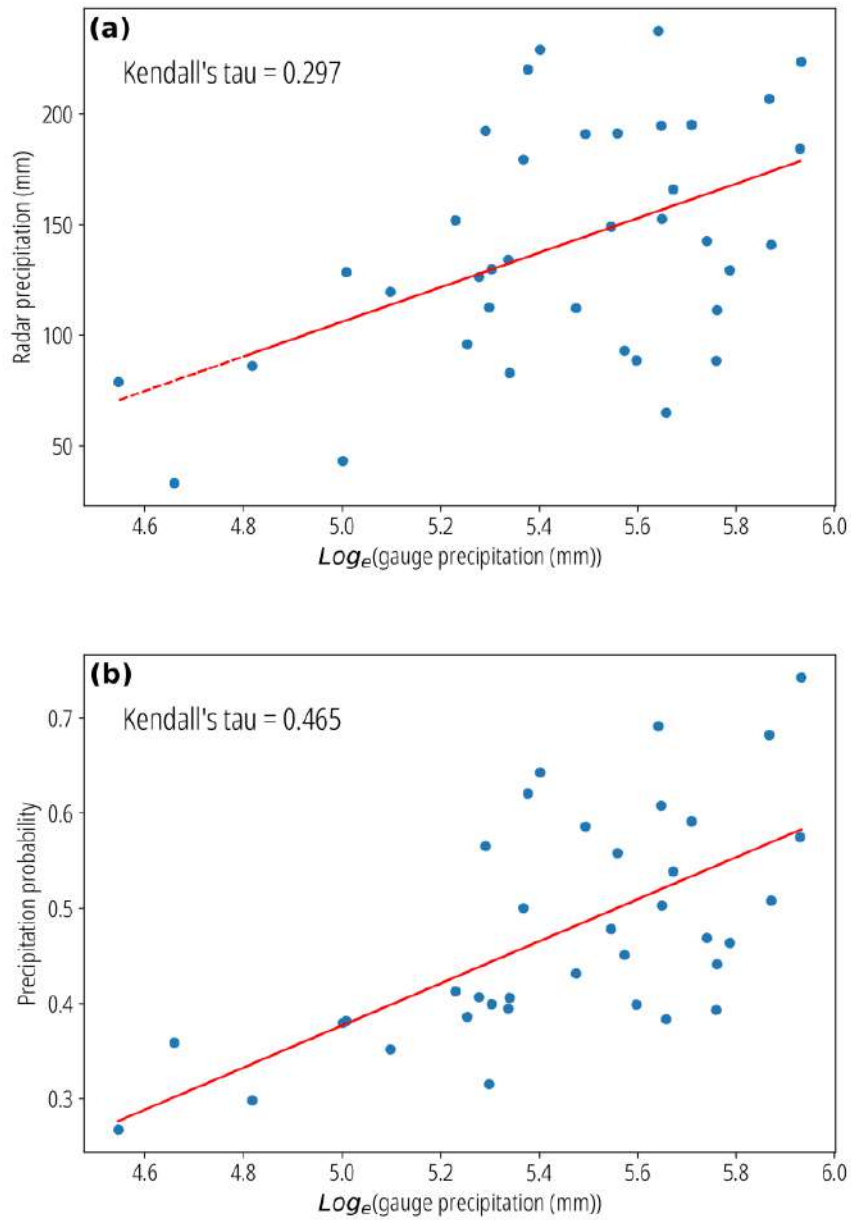


Figure 4: Scatter plots of radar precipitation (a) and joint membership probability (b) vs. log of gauge observed precipitation, **North region, 01/2018**

Table 3: Monthly correlation statistics: Kendall’s tau between radar precipitation and gauge observations and between Joint Membership Function (JMF) and gauges. The Residuals test columns show Shapiro-Wilk (SW) and Breusch-Pagan (BP) test for heteroscedasticity, where **bold numbers** emphasize low *p-values*, indicating that H_0 (normal, homoscedastic residuals) should be rejected. The final two columns present the β coefficients for each month to revert from JMF probability to precipitation (Subsection 3.2).

Study area	Month	Kendall’s tau		Residuals test		β coefficients	
		K-tau Radar	K-tau JMF	SW <i>p-value</i>	BP <i>p-value</i>	Slope	Intercept
North	01/2018	0.297	0.466	0.771	0.383	0.221	-0.728
North	10/2018	0.438	0.486	0.000	0.787	0.045	0.194
North	11/2018	0.641	0.610	0.825	0.479	0.110	-0.068
North	12/2018	0.152	0.533	0.906	0.142	0.169	-0.495
North	01/2019	0.162	0.406	0.307	0.313	0.079	0.005
South	01/2018	0.663	0.811	0.000	0.240	0.150	-0.136
South	10/2018	0.578	0.449	0.400	0.000	0.054	0.346
South	11/2018	0.554	0.596	0.033	0.313	0.149	-0.049
South	12/2018	0.406	0.765	0.099	0.022	0.134	0.124
South	01/2019	0.650	0.564	0.069	0.022	0.057	0.426

Table 4: Event (one day) correlation statistics

Study area	Event	Kendall’s tau	
		Radar	JMF
North	Dec. 7, 2018	0.33	0.38
North	Jan. 16, 2019	0.32	0.50
South	Oct. 25, 2018	0.60	0.61

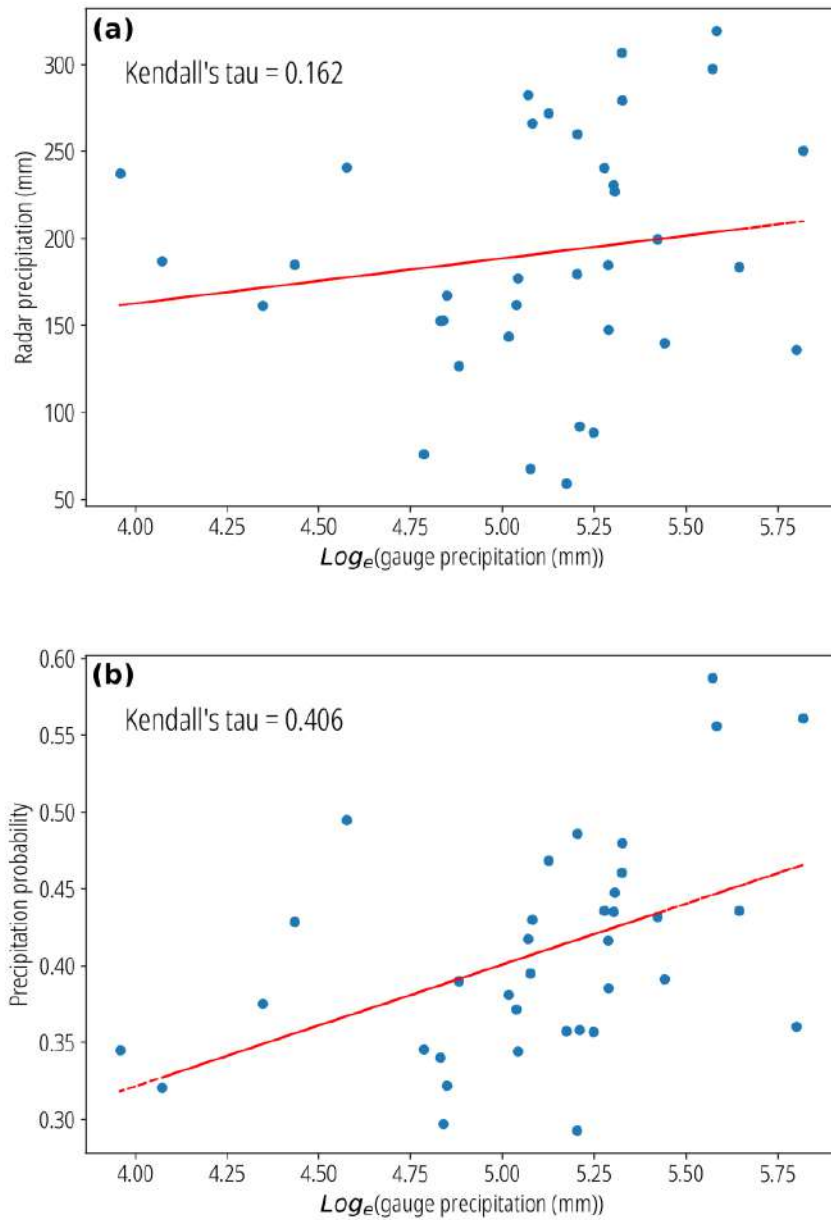


Figure 5: Scatter plots of radar precipitation (a) and joint membership probability (b) vs. log of gauge observed precipitation, **North region, 01/2019**

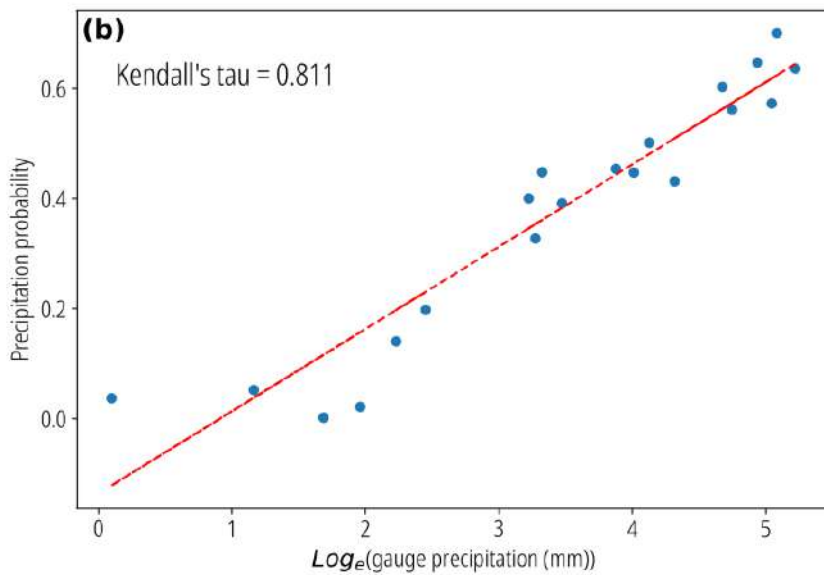
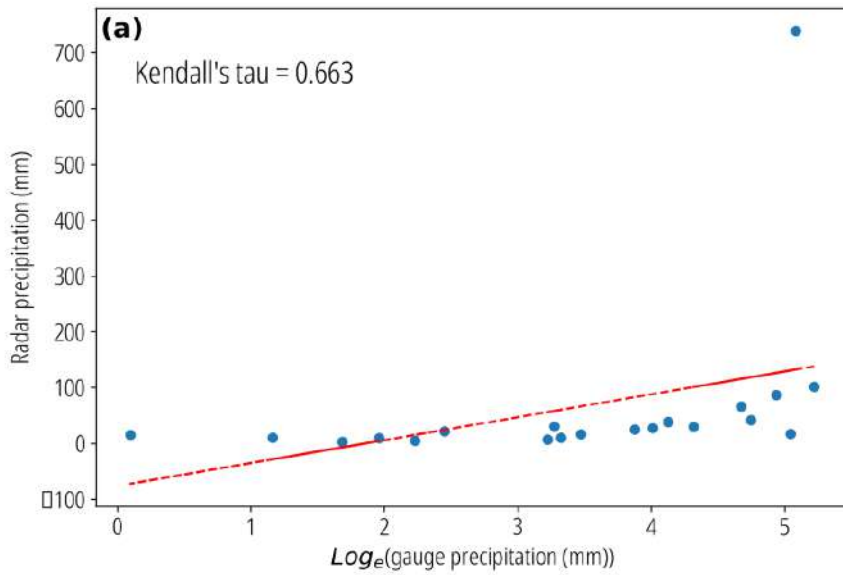


Figure 6: Scatter plots of radar precipitation (a) and joint membership probability (b) vs. log of gauge observed precipitation, **South region, 01/2018**

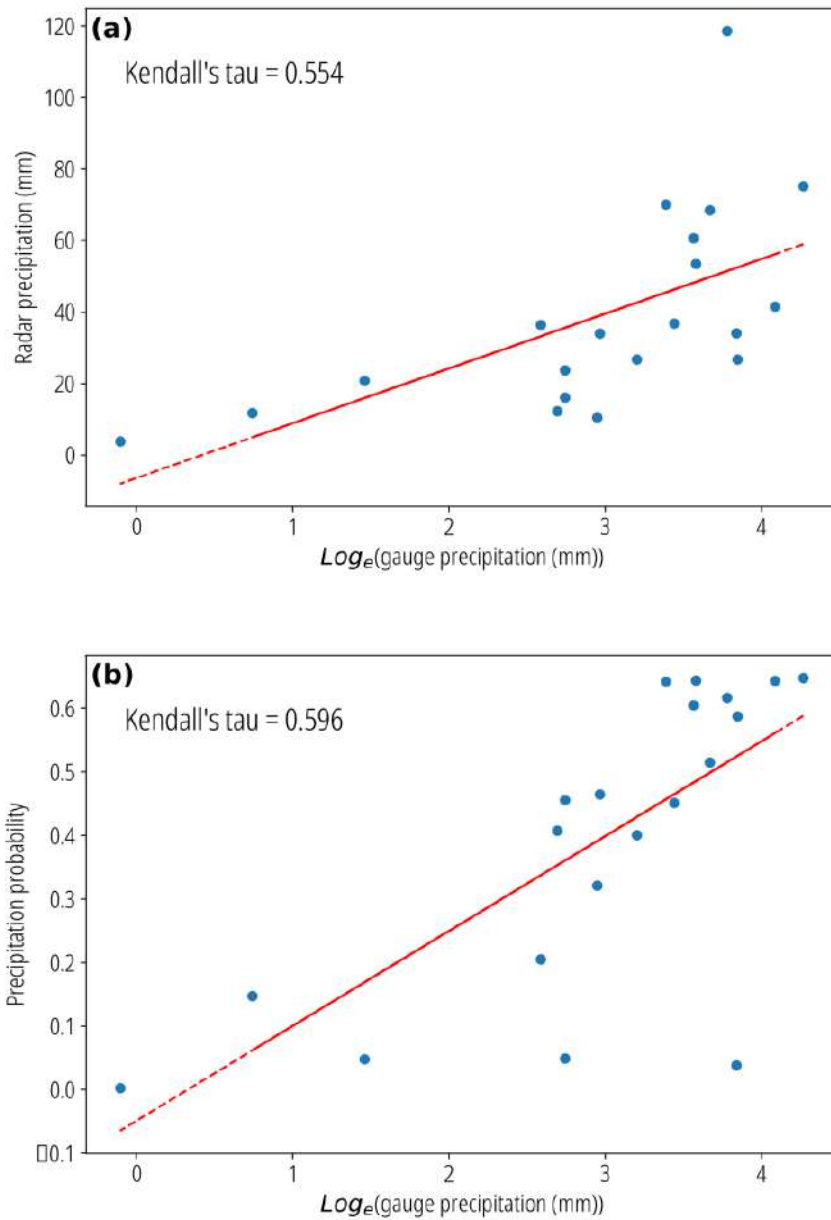


Figure 7: Scatter plots of radar precipitation (a) and joint membership probability (b) vs. log of gauge observed precipitation, **South region, 11/2018**

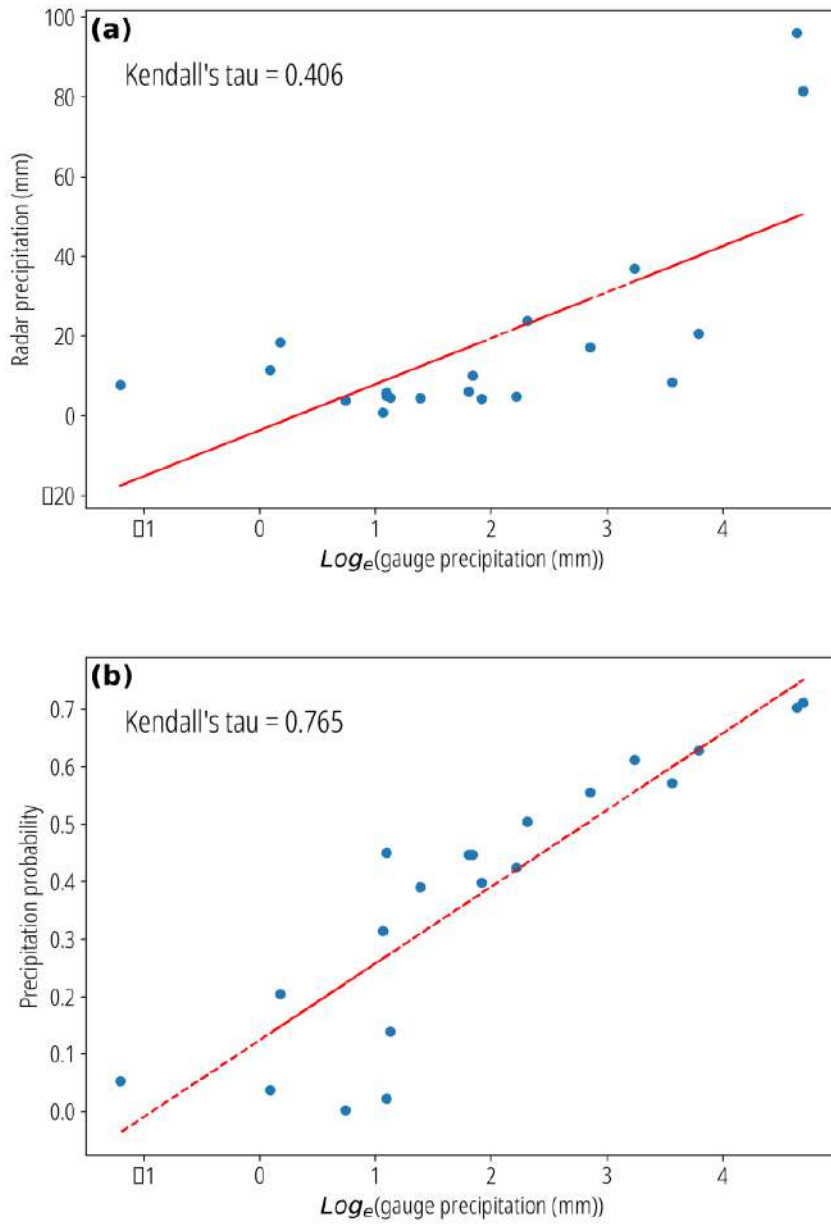


Figure 8: Scatter plots of radar precipitation (a) and joint membership probability (b) vs. log of gauge observed precipitation, **South region, 12/2018**

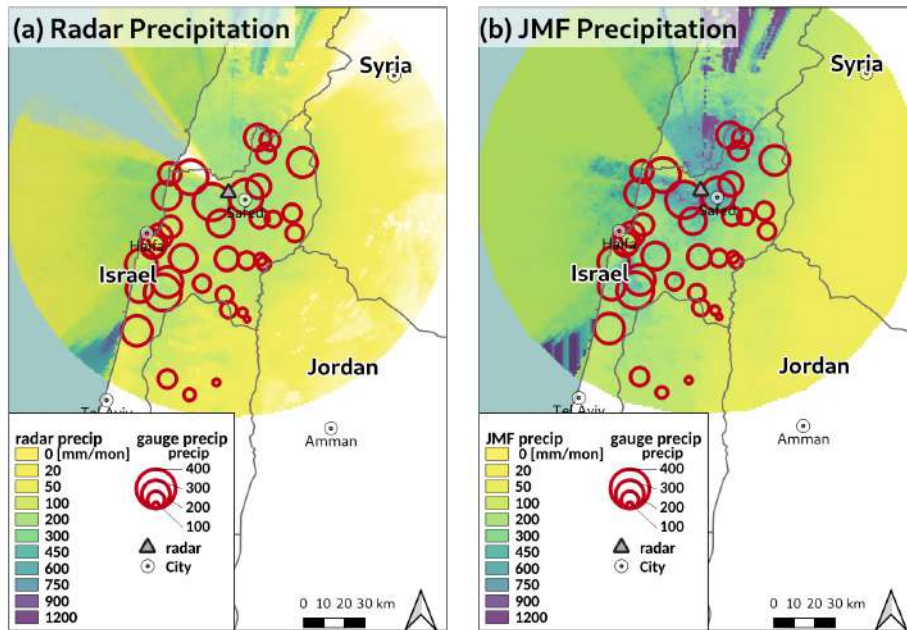


Figure 9: Precipitation maps, radar (a) and joint membership (b) precipitation distributions, North region, 01/2018

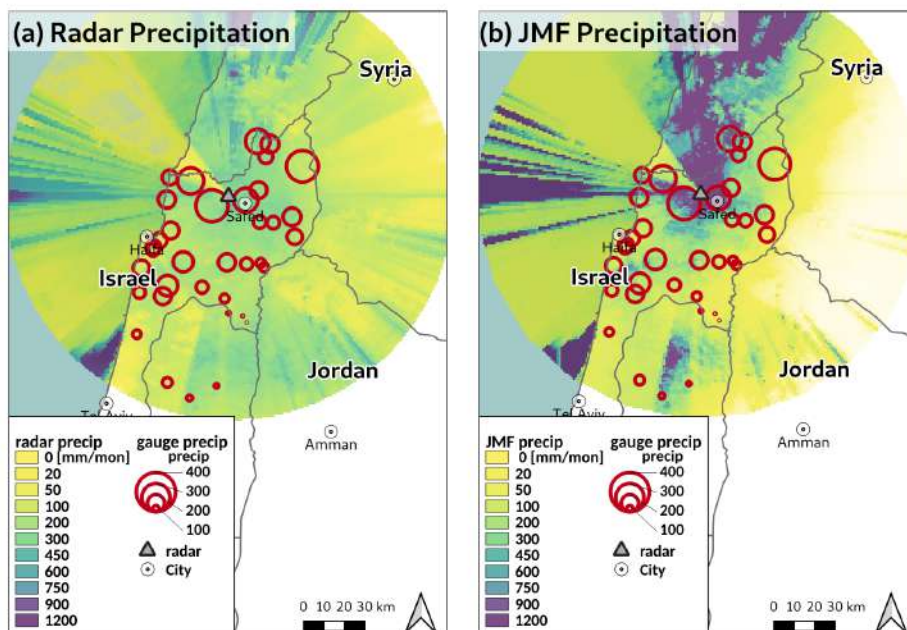


Figure 10: Precipitation maps, radar (a) and joint membership (b) precipitation distributions, North region, 01/2019

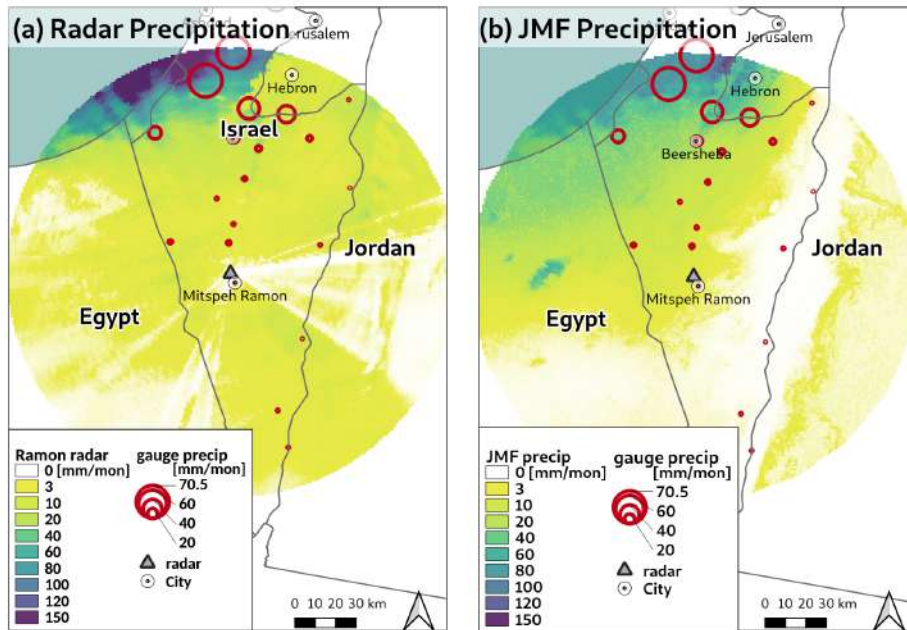


Figure 11: Precipitation maps, radar (a) and joint membership (b) precipitation distributions, South region, 12/2018

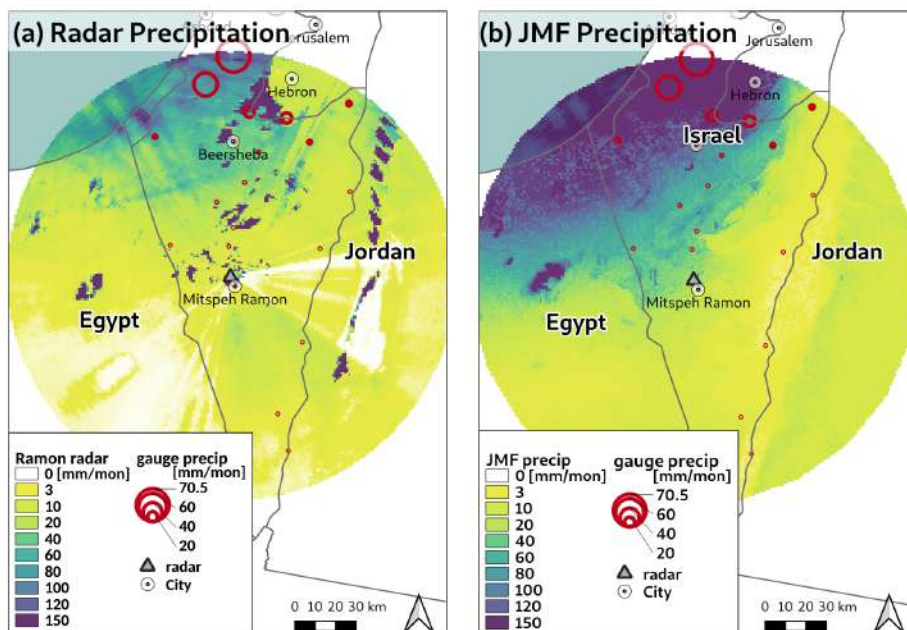


Figure 12: Precipitation maps, radar (a) and joint membership (b) precipitation distributions, South region, 01/2019

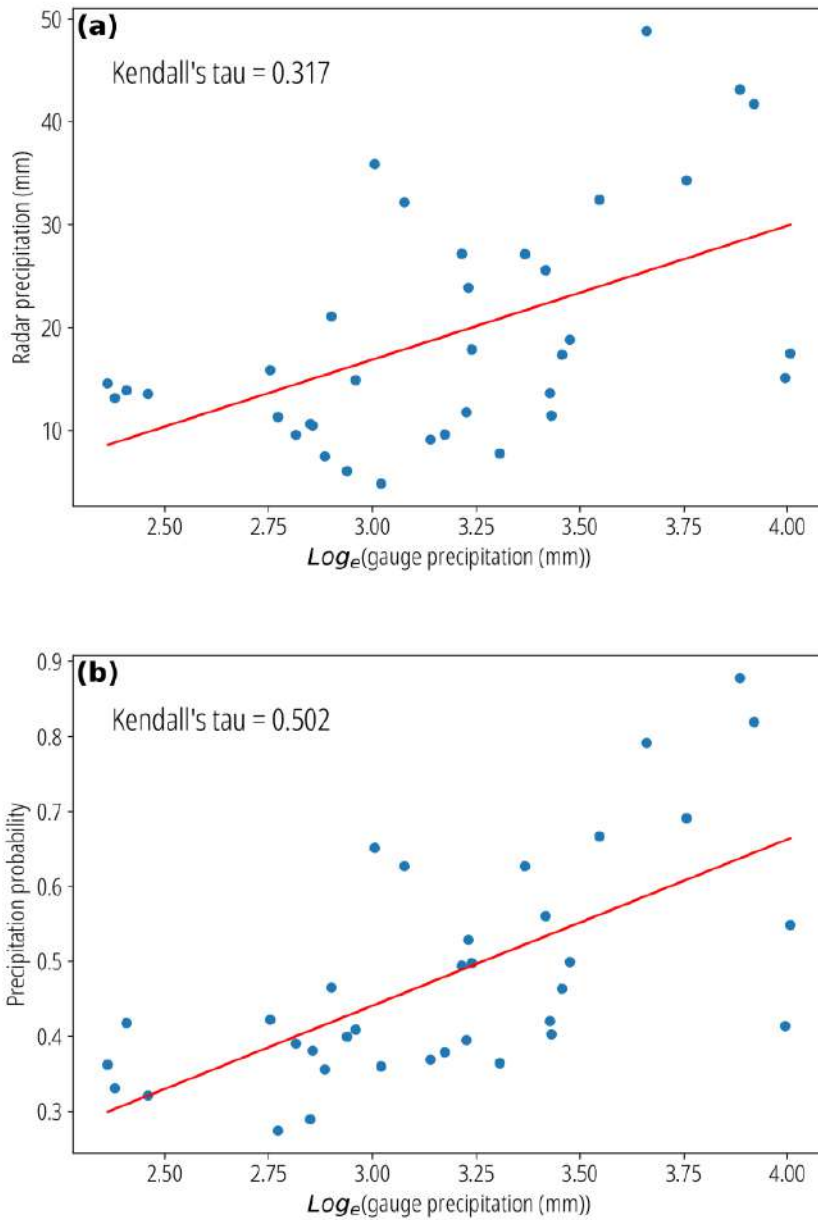


Figure 13: Single storm event scatter plots of radar precipitation (a) and joint membership probability (b) vs. log of gauge observed precipitation, **North region, 16/01/2019**

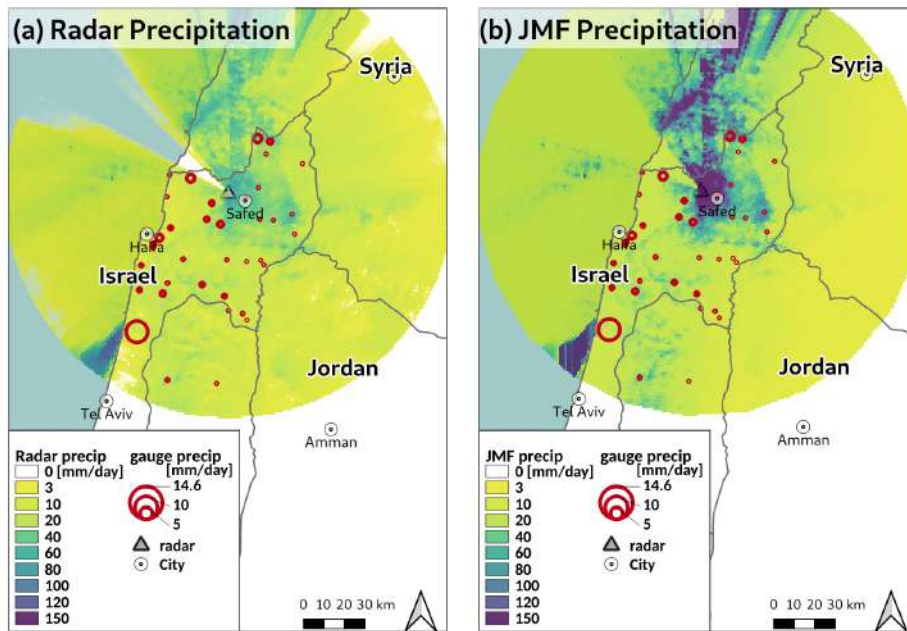


Figure 14: Single storm event precipitation maps, radar precipitation (a) and joint membership probability (b), North region, 16/01/2019

372 4. Discussion

373 4.1. Fuzzy method

374 This work produced improved precipitation maps from weather radar by applying
375 a fuzzy logic model using a set of location-based variables. Choice of this modeling
376 framework allowed flexibility in determining the spatial distribution of each variable (refer
377 to Section 2.2). The elevation MF, for example, was not represented by the simple above
378 sea level value. Rather a probability function assigned graduated probabilities to the
379 range of elevations, such that all low lying areas were represented by very low probability,
380 and all mountainous areas by high probability. In this way, the model enhanced the effect
381 of the elevation variable. Similarly, the distance from the coast MF was chosen such that
382 all areas within 100 km of the coast were assigned high probability, and all distant regions
383 near zero probability, reflecting the reality of the influence of distance from the sea in
384 the eastern Mediterranean.

385 The fuzzy logic approach also enabled adoption of synoptic classifications of storm
386 events that would not have been possible in other models. The MF for aspect allowed
387 transformation of the aspect azimuth to storm facing slopes. For each month in the
388 study period, the proportion of each synoptic class was tallied. Then, we determined
389 the direction of storm motion for each synoptic class, and matched that with aspect
390 azimuth to find storm facing pixels. Each pixel was assigned a probability, derived from
391 the proportion of synoptic events moving towards the pixel aspect. The results showed
392 that this variable had only a minor influence on the precipitation outcome, nevertheless
393 that level of influence in itself was appended to our composite of conclusions.

394 The original weather radar grids were also transformed by the radar MF to monthly
395 probability grids. In defining the radar MF as an “S” curve, with very low probability
396 at low rain depth, the model suppressed the misleading effects of radar uncertainty at
397 those low rain depth areas. Furthermore, at areas of high radar precipitation, the radar
398 MF reached probability of 1.0, thus enhancing areas where the radar grids were more
399 likely to be reliable.

400 4.2. Location-based variables

401 With the chosen set of location-based variables, and assigned MFs, a JMF was pro-
402 posed (Section 2.3 and equation (3)) as a sum of the MFs, each multiplied by a weight.
403 The vector of weights was determined by running an optimization function to find the
404 maximum correlation between gauge observations and the JMF probabilities at gauge
405 locations. The optimization function output essentially represented the influence of each
406 variable in the model. We found that, along with the original radar grids, distance from
407 the coast had the greatest influence in determining high correlation with gauge observa-
408 tions. This was true especially in the south, where the study area reached 200 km from
409 the coast.

410 The elevation MF was found to have a moderate influence in both northern and
411 southern regions. Our result aligns well with earlier research pointing to the correlation
412 between elevation and rainfall (Tang et al. (2018) and Lassegues (2018) are two recent
413 examples). It is interesting to note that we found slope and aspect had a minor influence,
414 and only in the southern study area, with an arid climate. Often slope and aspect are
415 highly correlated with elevation, so keeping both variables in a modeling framework might
416 lead to over-fitting. However in this case we found that slope and aspect had a minor
417 impact only in the southern region and no impact in the northern area, therefore that
418 concern of over-fitting could be put aside.

419 We associate the slight influence of slope and aspect in the arid region with rainfall
420 depth. Storms in the southern study area are often highly convective, fast moving from
421 the south, and with an intense rain rate for a short time, but small total rainfall depth.
422 In these cases both slope and aspect have some impact, due to orographic forcing. In the
423 northern study area, conversely, storms are often classified as a Cyprus low front, which
424 moves more slowly, and releases heavy precipitation over longer periods. In that case,
425 neither slope nor aspect influence the rain depth as precipitation is released throughout
426 the mountain areas.

427 A small number of papers, as far as the authors are aware, have examined the effect
428 of slope or aspect on precipitation, Sanchez-Moreno et al. (2014) being one example.
429 However that work was done on an island, with very unique weather behavior. Kitchen
430 et al. (1994), in their work on correcting weather radar for bright band effects, pointed
431 to wind direction and speed as factors insofar as they influence orographic forcing. They
432 refer back to Hill (1983) who reported higher rainfall over hills due to orographic effects
433 and analyzed wind direction in this context. These previous works notwithstanding, in-
434 clusion of slope and aspect in the current work constitutes an innovation. Furthermore,
435 the collection of location-based variables examined here has not, to the best of our knowl-
436 edge, been examined together before. Most research in modeling precipitation chooses
437 meteorological variables, and possibly elevation, as secondary inputs to geostatistic pro-
438 cedures such as kriging with external drift. This research merges several location-based
439 variables that, as seen in the JMF weights, influence precipitation, and allow the model
440 to improve weather radar precipitation grids.

441 *4.3. Improved precipitation maps*

442 Reviewing the correlation results in Table 3, certain months show improvement: i.e.
443 January, 2018, and December 2018. Contrary to those months, October and November
444 stand out with little improvement and in one case (October, 2018) lower correlation after
445 applying the fuzzy model. We attribute the poor performance of the model for certain
446 months to high localized rainfall variance over the month. The location-based based
447 model cannot deal with extreme rainfall variance at given locations over an aggregation
448 period. Since the variables are all spatially based, if rainfall changes dramatically over

449 the aggregation period, at a certain location, the model fails. This limitation is revealed
 450 in the eastern Mediterranean during transition seasons such as October-November and
 451 March-April. During these months rainfall variance at each gauge can be much larger
 452 than the mean precipitation for the month, confounding this location-based based model.

453 To test this hypothesis, the mean (μ) and standard deviation (σ) of gauge observed
 454 precipitation for each month at the individual validation gauges were obtained. Then
 455 the coefficient of variation (CV) ($CV = \sigma/\mu$) was calculated. Average CV of all gauges
 for the study periods are presented in Table 5:

Study area	Month	CV
North	Nov. 2018	1.46
North	Dec. 2018	1.29
North	Jan. 2019	0.89
South	Jan. 2018	1.04
South	Nov. 2018	1.24
South	Dec. 2018	1.09

Table 5: Average coefficient of variation for the study periods. The **bold cell** emphasizes a study period with high localized rainfall variance.

456

457 The high coefficient of variation (averaged over all gauges) during November 2018 in
 458 the northern region revealed that during that month there were erratic rainfall depths
 459 throughout the month, unrelated to elevation, distance from the coast, etc., thus ex-
 460 plaining the poor correlation of the model for this month (in Table 3). This result
 461 highlighted a limitation of the location-based based model: the model is appropriate for
 462 "well-behaved" aggregation periods, i.e. periods when precipitation has a low coefficient
 463 of variation.

464 For those months showing improved precipitation maps, it is worthwhile to point out
 465 specific regions where the precipitation grid improved, and postulate the reason for the
 466 improvement. Referring to the pair of maps in Figure 9 for January 2018, in the north,
 467 it is clear from the uniform size of the blue, circular gauge markers that the monthly
 468 precipitation was heavy throughout the center of this study area for that month. However
 469 the radar (panel (a)) does not correctly capture that uniform distribution. Some regions
 470 far from the radar, in the high elevation to the north east and in the southern edge are
 471 light green to yellow (low rainfall depth). The improved JMF precipitation grid, in the
 472 right panel does show increased rain depth both in the center and north, probably due
 473 to high elevation in both of these areas, and captured by the elevation MF.

474 Similarly, in Figure 12 gauges at the northern edge of the southern study area, close
 475 to the coast, show fairly high precipitation for the month. The radar image incorrectly
 476 shows this area as light green. The JMF precipitation grid, however, corrects the rain
 477 depth, showing this area as dark-green to blue. The correction is most likely due to the
 478 proximity to the sea, encapsulated in the distance to coast MF.

479 4.4. Applicability

480 Flood forecasting requires highly accurate precipitation grids that can be input into a
481 hydro-meteorological model in real time. The variables included in the fuzzy logic model
482 proposed here can all be made available in advance or in real time. The static location-
483 based factors are prepared once in advance. Even though the aspect variable varies
484 month by month, dependent on the proportion of synoptic classes, those proportions,
485 as described in Section 2.2, are available from past research. Thus the aspect MF can
486 also be prepared in advance for all months of the year. The only varying component
487 of the model is the weather radar grid. Outputs from weather radar are often available
488 publicly and in real time from many national meteorological services. Therefore the
489 option to run the proposed model and produce improved precipitation grids in real time
490 is operationally possible.

491 5. Conclusion

492 The fuzzy logic approach presented herein successfully produced spatially distributed
493 precipitation grids from weather radar and location-based variables alone. The method
494 was applied to two eastern Mediterranean study regions, over four winter months, and
495 at both monthly and daily aggregation periods. Four variables were merged with the
496 radar precipitation grid: elevation, distance from coast, slope and aspect. Each of these
497 variables was expressed as a MF probability. Then a JMF of additive terms was applied,
498 where each term was the product of one variable probability multiplied by its weight
499 coefficient. This JMF produced precipitation probability grids for both study regions.
500 Gauge observations from 57 locations throughout the study regions served to validate
501 the model results.

502 Our finds indicate:

- 503 1. The JMF derived precipitation grids were better correlated to gauge observations
504 than the original radar;
- 505 2. JMF probabilities were linearly correlated to \log_e of the gauge observations;
- 506 3. The two most influential variables were distance from the coast and the original
507 weather radar grid;
- 508 4. Elevation had a moderate influence in both climate regions;
- 509 5. Slope and aspect (storm facing slopes) had a minor influence only in the southern
510 arid region;
- 511 6. The model performed poorly during aggregation periods when precipitation dis-
512 played a high localized coefficient of variation.

513 6. Acknowledgements

514 The authors thank the Israeli Meteorological Service for their effort in offering public
515 access to their climate data. We also thank Dr. Nir Sapir from the University of Haifa,

516 Department of Evolutionary and Environmental Biology, and his research staff for their
517 help in obtaining the radar data files.

518 This research was partially funded by DFG/IMAP grant GZ: KU2090/7-2, AOBJ:
519 633213.

520 References

- 521 Adhikary, S.K., Muttill, N., Yilmaz, A.G., 2017. Cokriging for enhanced spatial interpolation of rainfall
522 in two Australian catchments. *Hydrological Processes* 31, 2143–2161. URL: <http://doi.wiley.com/10.1002/hyp.11163>, doi:10.1002/hyp.11163.
- 524 Agboola, A., Gabriel, A., Aliyu, E., Alese, B., 2015. Development of a Fuzzy Logic Based Rainfall
525 Prediction Model. *International Journal of Engineering and Technology* 3.
- 526 Alpert, P., Osetinsky, I., Ziv, B., Shafir, H., 2004. Semi-objective classification for daily synoptic systems:
527 application to the eastern Mediterranean climate change. *International Journal of Climatology* 24,
528 1001–1011. URL: <http://doi.wiley.com/10.1002/joc.1036>, doi:10.1002/joc.1036.
- 529 Arazi, A., Sharon, D., Khain, A., Huss, A., Mahrer, Y., 1997. THE WINDFIELD AND RAINFALL
530 DISTRIBUTION INDUCED WITHIN A SMALL VALLEY: FIELD OBSERVATIONS AND 2-D NU-
531 MERICAL MODELLING. *Boundary-Layer Meteorology* 83, 349–374. URL: <http://link.springer.com/10.1023/A:1000243312103>, doi:10.1023/A:1000243312103.
- 533 Asklany, S.A., Elhelow, K., Youssef, I., Abd El-wahab, M., 2011. Rainfall events prediction using
534 rule-based fuzzy inference system. *Atmospheric Research* 101, 228–236. URL: <http://linkinghub.elsevier.com/retrieve/pii/S0169809511000640>, doi:10.1016/j.atmosres.2011.02.015.
- 536 Berenguer, M., Sempere-Torres, D., Corral, C., Sánchez-Diezma, R., 2006. A Fuzzy Logic Technique
537 for Identifying Nonprecipitating Echoes in Radar Scans. *J. Atmos. Oceanic Technol.* 23, 1157–1180.
538 URL: <http://journals.ametsoc.org/doi/abs/10.1175/JTECH1914.1>, doi:10.1175/JTECH1914.1.
- 539 Berndt, C., Rabiei, E., Haberlandt, U., 2014. Geostatistical merging of rain gauge and radar data
540 for high temporal resolutions and various station density scenarios. *Journal of Hydrology* 508,
541 88–101. URL: <http://linkinghub.elsevier.com/retrieve/pii/S0022169413007476>, doi:10.1016/j.jhydrol.2013.10.028.
- 543 Besalatpour, A., Hajabbasi, M.A., Ayoubi, S., Afyuni, M., Jalalian, A., Schulin, R., 2012. Soil shear
544 strength prediction using intelligent systems: artificial neural networks and an adaptive neuro-fuzzy
545 inference system. *Soil Science and Plant Nutrition* 58, 149–160. URL: <http://www.tandfonline.com/doi/abs/10.1080/00380768.2012.661078>, doi:10.1080/00380768.2012.661078.
- 547 Carrera-Hernández, J., Gaskin, S., 2007. Spatio temporal analysis of daily precipitation and temperature
548 in the Basin of Mexico. *Journal of Hydrology* 336, 231–249. URL: <http://linkinghub.elsevier.com/retrieve/pii/S0022169406006718>, doi:10.1016/j.jhydrol.2006.12.021.
- 550 Cecinati, F., Rico-Ramirez, M.A., Heuvelink, G.B., Han, D., 2017. Representing radar rainfall uncer-
551 tainty with ensembles based on a time-variant geostatistical error modelling approach. *Journal of Hy-*
552 *drology* 548, 391–405. URL: <http://linkinghub.elsevier.com/retrieve/pii/S0022169417301324>,
553 doi:10.1016/j.jhydrol.2017.02.053.
- 554 Chumchean, S., Sharma, A., Seed, A., 2003. Radar rainfall error variance and its impact on radar rainfall
555 calibration. *Physics and Chemistry of the Earth, Parts A/B/C* 28, 27–39. URL: <http://linkinghub.elsevier.com/retrieve/pii/S1474706503000056>, doi:10.1016/S1474-7065(03)00005-6.
- 557 Cohen, S., Svoray, T., Laronne, J.B., Alexandrov, Y., 2008. Fuzzy-based dynamic soil erosion
558 model (FuDSEM): Modelling approach and preliminary evaluation. *Journal of Hydrology* 356,
559 185–198. URL: <http://linkinghub.elsevier.com/retrieve/pii/S0022169408001820>, doi:10.1016/j.jhydrol.2008.04.010.
- 561 Colli, M., Lanza, L., La Barbera, P., 2013. Performance of a weighing rain gauge under laboratory
562 simulated time-varying reference rainfall rates. *Atmospheric Research* 131, 3–12. URL: <http://linkinghub.elsevier.com/retrieve/pii/S016980951300121X>, doi:10.1016/j.atmosres.2013.04.006.
- 564 006.
- 565 Comber, A., Fisher, P., Brunson, C., Khmag, A., 2012. Spatial analysis of remote sensing image
566 classification accuracy. *Remote Sensing of Environment* 127, 237–246. URL: <http://linkinghub.elsevier.com/retrieve/pii/S0034425712003598>, doi:10.1016/j.rse.2012.09.005.
- 567 005.
- 568 Daly, C., Neilson, R., Phillips, D., 1992. A Statistical-Topographic Model for Mapping Clima-
569 tological Precipitation over Mountainous Terrain. *Journal of Applied Meteorology* 33, 140–

570 158. URL: [https://journals.ametsoc.org/doi/pdf/10.1175/1520-0450%281994%29033%3C0140%](https://journals.ametsoc.org/doi/pdf/10.1175/1520-0450%281994%29033%3C0140%3AAASTMFM%3E2.O.CO%3B2)
571 [3AAASTMFM%3E2.O.CO%3B2](https://journals.ametsoc.org/doi/pdf/10.1175/1520-0450%281994%29033%3C0140%3AAASTMFM%3E2.O.CO%3B2).

572 Daniels, E.E., Lenderink, G., Hutjes, R.W.A., Holtslag, A.A.M., 2014. Spatial precipitation patterns
573 and trends in The Netherlands during 1951-2009: SPATIAL PRECIPITATION PATTERNS AND
574 TRENDS. *International Journal of Climatology* 34, 1773–1784. URL: [http://doi.wiley.com/10.](http://doi.wiley.com/10.1002/joc.3800)
575 [1002/joc.3800](http://doi.wiley.com/10.1002/joc.3800), doi:10.1002/joc.3800.

576 Dieulin, C., Mahé, G., Paturel, J.E., Ejjiyar, S., Trambly, Y., Rouché, N., EL Mansouri, B., 2019.
577 A New 60-year 1940/1999 Monthly-Gridded Rainfall Data Set for Africa. *Water* 11, 387. URL:
578 <http://www.mdpi.com/2073-4441/11/2/387>, doi:10.3390/w11020387.

579 Dufton, D.R.L., Collier, C.G., 2015. Fuzzy logic filtering of radar reflectivity to remove non-
580 meteorological echoes using dual polarization radar moments. *Atmos. Meas. Tech.* 8, 3985–4000.
581 URL: <https://www.atmos-meas-tech.net/8/3985/2015/>, doi:10.5194/amt-8-3985-2015.

582 Foody, G.M., 1996. Approaches for the production and evaluation of fuzzy land cover classifications
583 from remotely-sensed data. *International Journal of Remote Sensing* 17, 1317–1340. URL: [http:](http://www.tandfonline.com/doi/abs/10.1080/01431169608948706)
584 [//www.tandfonline.com/doi/abs/10.1080/01431169608948706](http://www.tandfonline.com/doi/abs/10.1080/01431169608948706), doi:10.1080/01431169608948706.

585 Foody, G.M., 2002. Status of land cover classification accuracy assessment. *Remote Sensing of En-*
586 *vironment* 80, 185–201. URL: <http://linkinghub.elsevier.com/retrieve/pii/S0034425701002954>,
587 doi:10.1016/S0034-4257(01)00295-4.

588 Giap, Q.H., 2014. Interactive diagnosis for a grid network of rain gauges using fuzzy reasoning. *Engi-*
589 *neering Applications of Artificial Intelligence* , 15.

590 Goovaerts, P., 2000. Geostatistical approaches for incorporating elevation into the spatial interpolation
591 of rainfall. *Journal of Hydrology* 228, 113–129. URL: [http://linkinghub.elsevier.com/retrieve/](http://linkinghub.elsevier.com/retrieve/pii/S002216940000144X)
592 [pii/S002216940000144X](http://linkinghub.elsevier.com/retrieve/pii/S002216940000144X), doi:10.1016/S0022-1694(00)00144-X.

593 Guan, H., Wilson, J.L., Makhnin, O., 2005. Geostatistical Mapping of Mountain Precipitation Incorpor-
594 ating Autosearched Effects of Terrain and Climatic Characteristics. *J. Hydrometeor.* 6, 1018–1031.
595 URL: <https://journals.ametsoc.org/doi/full/10.1175/JHM448.1>, doi:10.1175/JHM448.1.

596 Guifrída, A., Nagi, R., 1998. Fuzzy set theory applications in production management research: a
597 literature survey. *Journal of Intelligent Manufacturing* 9, 18.

598 Hayward, D., Clarke, R.T., 1996. Relationship between rainfall, altitude and distance from the sea
599 in the Freetown Peninsula, Sierra Leone. *Hydrological Sciences Journal* 41, 377–384. URL: [https:](https://www.tandfonline.com/doi/full/10.1080/02626669609491509)
600 [//www.tandfonline.com/doi/full/10.1080/02626669609491509](https://www.tandfonline.com/doi/full/10.1080/02626669609491509), doi:10.1080/02626669609491509.

601 Heistermann, M., Jacobi, S., Pfaff, T., 2013. Technical Note: An open source library for processing
602 weather radar data (wradlib). *Hydrology and Earth System Sciences* 17, 863–871. URL: [http:](http://www.hydrol-earth-syst-sci.net/17/863/2013/)
603 [//www.hydrol-earth-syst-sci.net/17/863/2013/](http://www.hydrol-earth-syst-sci.net/17/863/2013/), doi:10.5194/hess-17-863-2013.

604 Hill, F.F., 1983. The use of average annual rainfall to derive estimates of orographic enhancement of
605 frontal rain over England and Wales for different wind directions. *J. Climatol.* 3, 113–129. URL:
606 <http://doi.wiley.com/10.1002/joc.3370030202>, doi:10.1002/joc.3370030202.

607 Hong, H., Panahi, M., Shirzadi, A., Ma, T., Liu, J., Zhu, A.X., Chen, W., Kougiyas, I., Kazakis, N.,
608 2018. Flood susceptibility assessment in Hengfeng area coupling adaptive neuro-fuzzy inference system
609 with genetic algorithm and differential evolution. *Science of The Total Environment* 621, 1124–
610 1141. URL: <https://linkinghub.elsevier.com/retrieve/pii/S0048969717328176>, doi:10.1016/j.
611 [scitotenv.2017.10.114](https://linkinghub.elsevier.com/retrieve/pii/S0048969717328176).

612 Hundecha, Y., Bardossy, A., Werner, H.W., 2001. Development of a fuzzy logic-based rainfall-runoff
613 model. *Hydrological Sciences Journal* 46, 363–376. URL: [http://www.tandfonline.com/doi/abs/10.](http://www.tandfonline.com/doi/abs/10.1080/02626660109492832)
614 [1080/02626660109492832](http://www.tandfonline.com/doi/abs/10.1080/02626660109492832), doi:10.1080/02626660109492832.

615 Jang, J.S., 1993. ANFIS: adaptive-network-based fuzzy inference system. *IEEE Trans. Syst., Man, Cy-*
616 *bern.* 23, 665–685. URL: <http://ieeexplore.ieee.org/document/256541/>, doi:10.1109/21.256541.

617 Jasiewicz, J., 2011. A new GRASS GIS fuzzy inference system for massive data analysis. *Com-*
618 *puters & Geosciences* 37, 1525–1531. URL: [https://linkinghub.elsevier.com/retrieve/pii/](https://linkinghub.elsevier.com/retrieve/pii/S0098300410003171)
619 [S0098300410003171](https://linkinghub.elsevier.com/retrieve/pii/S0098300410003171), doi:10.1016/j.cageo.2010.09.008.

- 620 Kadmon, R., Danin, A., 1999. Distribution of plant species in Israel in relation to spatial variation in
621 rainfall. *Journal of Vegetation Science* 10, 421–432. URL: [https://onlinelibrary.wiley.com/doi/](https://onlinelibrary.wiley.com/doi/abs/10.2307/3237071)
622 [abs/10.2307/3237071](https://onlinelibrary.wiley.com/doi/abs/10.2307/3237071), doi:10.2307/3237071.
- 623 Kebaili Bargaoui, Z., Chebbi, A., 2009. Comparison of two kriging interpolation methods applied to
624 spatiotemporal rainfall. *Journal of Hydrology* 365, 56–73. URL: [http://linkinghub.elsevier.com/](http://linkinghub.elsevier.com/retrieve/pii/S0022169408005726)
625 [retrieve/pii/S0022169408005726](http://linkinghub.elsevier.com/retrieve/pii/S0022169408005726), doi:10.1016/j.jhydrol.2008.11.025.
- 626 Kidd, C., Becker, A., Huffman, G.J., Muller, C.L., Joe, P., Skofronick-Jackson, G., Kirschbaum, D.B.,
627 2017. So, How Much of the Earth’s Surface Is Covered by Rain Gauges? *Bulletin of the American Me-*
628 *teorological Society* 98, 69–78. URL: [http://journals.ametsoc.org/doi/10.1175/BAMS-D-14-00283.](http://journals.ametsoc.org/doi/10.1175/BAMS-D-14-00283.1)
629 [1](http://journals.ametsoc.org/doi/10.1175/BAMS-D-14-00283.1), doi:10.1175/BAMS-D-14-00283.1.
- 630 Kim, B.S., Hong, J.B., Kim, H.S., Yoon, S.Y., 2007. Combining Radar and Rain Gauge Rainfall Esti-
631 mates for Flood Forecasting Using Conditional Merging Method, *American Society of Civil Engineers*.
632 pp. 1–16. URL: <http://ascelibrary.org/doi/10.1061/40927%28243%29414>, doi:10.1061/40927(243)
633 [414](http://ascelibrary.org/doi/10.1061/40927%28243%29414).
- 634 Kirstetter, P.E., Delrieu, G., Boudevillain, B., Obled, C., 2010. Toward an error model for radar
635 quantitative precipitation estimation in the Cévennes–Vivarais region, France. *Journal of Hy-*
636 *drology* 394, 28–41. URL: <http://linkinghub.elsevier.com/retrieve/pii/S002216941000020X>,
637 [doi:10.1016/j.jhydrol.2010.01.009](http://linkinghub.elsevier.com/retrieve/pii/S002216941000020X).
- 638 Kitchen, M., Brown, R., Davies, A.G., 1994. Real-time correction of weather radar data for the effects
639 of bright band, range and orographic growth in widespread precipitation. *Q.J Royal Met. Soc.* 120,
640 1231–1254. URL: <http://doi.wiley.com/10.1002/qj.49712051906>, doi:10.1002/qj.49712051906.
- 641 Klir, G., Yuan, B., 1995. *Fuzzy Sets and Fuzzy Logic Theory and Ap-*
642 *plications*. Prentice-Hall Inc. URL: [https://www.scribd.com/doc/50284358/](https://www.scribd.com/doc/50284358/Fuzzy-Sets-and-Fuzzy-Logic-Theory-and-Applications-George-j-Klir-Bo-Yuan)
643 [Fuzzy-Sets-and-Fuzzy-Logic-Theory-and-Applications-George-j-Klir-Bo-Yuan](https://www.scribd.com/doc/50284358/Fuzzy-Sets-and-Fuzzy-Logic-Theory-and-Applications-George-j-Klir-Bo-Yuan).
- 644 Kottek, M., Grieser, J., Beck, C., Rudolf, B., Rubel, F., 2006. World Map of the Köppen-Geiger climate
645 classification updated. *Meteorologische Zeitschrift* 15, 259–263. URL: [http://dx.doi.org/10.1127/](http://dx.doi.org/10.1127/0941-2948/2006/0130)
646 [0941-2948/2006/0130](http://dx.doi.org/10.1127/0941-2948/2006/0130), doi:10.1127/0941-2948/2006/0130.
- 647 Krajewski, W., Smith, J., 2002. Radar hydrology: rainfall estimation. *Advances in Water Resources*
648 25, 1387–1394. URL: <http://linkinghub.elsevier.com/retrieve/pii/S0309170802000623>, doi:10.
649 [1016/S0309-1708\(02\)00062-3](http://linkinghub.elsevier.com/retrieve/pii/S0309170802000623).
- 650 Krause, J.M., 2016. A Simple Algorithm to Discriminate between Meteorological and Nonmeteo-
651 rological Radar Echoes. *Journal of Atmospheric and Oceanic Technology* 33, 1875–1885. URL:
652 <http://journals.ametsoc.org/doi/10.1175/JTECH-D-15-0239.1>, doi:10.1175/JTECH-D-15-0239.1.
- 653 Lassegues, P., 2018. Daily and climatological fields of precipitation over the western Alps with a high
654 density network for the period of 1990–2012. *Theoretical and Applied Climatology* 131, 1–17. URL:
655 <http://link.springer.com/10.1007/s00704-016-1954-z>, doi:10.1007/s00704-016-1954-z.
- 656 Ly, S., Charles, C., Degré, A., 2013. Different methods for spatial interpolation of rainfall data for
657 operational hydrology and hydrological modeling at watershed scale. A review. *Biotechnol. Agron.*
658 *Soc. Environ.* , 15.
- 659 Makarieva, A.M., Gorshkov, V.G., Li, B.L., 2009. Precipitation on land versus distance from the
660 ocean: Evidence for a forest pump of atmospheric moisture. *Ecological Complexity* 6, 302–
661 307. URL: <https://linkinghub.elsevier.com/retrieve/pii/S1476945X08000834>, doi:10.1016/j.
662 [ecocom.2008.11.004](https://linkinghub.elsevier.com/retrieve/pii/S1476945X08000834).
- 663 Marra, F., Morin, E., 2018. Autocorrelation structure of convective rainfall in semiarid-arid climate de-
664 rived from high-resolution X-Band radar estimates. *Atmospheric Research* 200, 126–138. URL: <http://linkinghub.elsevier.com/retrieve/pii/S0169809517309936>, doi:10.1016/j.atmosres.2017.09.
665 [020](http://linkinghub.elsevier.com/retrieve/pii/S0169809517309936).
- 666 McKee, J.L., Binns, A.D., 2016. A review of gauge–radar merging methods for quantitative pre-
668 cipitation estimation in hydrology. *Canadian Water Resources Journal / Revue canadienne des*
669 *ressources hydriques* 41, 186–203. URL: <http://www.tandfonline.com/doi/full/10.1080/07011784>.

670 2015.1064786, doi:10.1080/07011784.2015.1064786.

671 Men, B., Long, R., Li, Y., Liu, H., Tian, W., Wu, Z., 2017. Combined Forecasting of Rainfall Based on
672 Fuzzy Clustering and Cross Entropy. *Entropy* 19, 694. URL: [http://www.mdpi.com/1099-4300/19/](http://www.mdpi.com/1099-4300/19/12/694)
673 [12/694](http://www.mdpi.com/1099-4300/19/12/694), doi:10.3390/e19120694.

674 Merz, B., Aerts, J., Arnbjerg-Nielsen, K., Baldi, M., Becker, A., Bichet, A., Blöschl, G., Bouwer,
675 L.M., Brauer, A., Cioffi, F., Delgado, J.M., Gocht, M., Guzzetti, F., Harrigan, S., Hirschboeck,
676 K., Kilsby, C., Kron, W., Kwon, H.H., Lall, U., Merz, R., Nissen, K., Salvatti, P., Swierczynski,
677 T., Ulbrich, U., Viglione, A., Ward, P.J., Weiler, M., Wilhelm, B., Nied, M., 2014. Floods and
678 climate: emerging perspectives for flood risk assessment and management. *Natural Hazards and Earth*
679 *System Science* 14, 1921–1942. URL: <http://www.nat-hazards-earth-syst-sci.net/14/1921/2014/>,
680 doi:10.5194/nhess-14-1921-2014.

681 Morin, E., Gabella, M., 2007. Radar-based quantitative precipitation estimation over Mediterranean
682 and dry climate regimes. *Journal of Geophysical Research* 112. URL: [http://doi.wiley.com/10.](http://doi.wiley.com/10.1029/2006JD008206)
683 [1029/2006JD008206](http://doi.wiley.com/10.1029/2006JD008206), doi:10.1029/2006JD008206.

684 Morin, E., Krajewski, W.F., Goodrich, D.C., Gao, X., Sorooshian, S., 2003. Estimating rainfall intensities
685 from weather radar data: The scale-dependency problem. *Journal of Hydrometeorology* 4, 782–
686 797. URL: [http://journals.ametsoc.org/doi/abs/10.1175/1525-7541\(2003\)004%3C0782:ERIFWR%](http://journals.ametsoc.org/doi/abs/10.1175/1525-7541(2003)004%3C0782:ERIFWR%3E2.0.CO;3B2)
687 [3E2.0.CO;3B2](http://journals.ametsoc.org/doi/abs/10.1175/1525-7541(2003)004%3C0782:ERIFWR%3E2.0.CO;3B2).

688 Neteler, M., Bowman, M.H., Landa, M., Metz, M., 2012. GRASS GIS: A multi-purpose open source
689 GIS. *Environmental Modelling & Software* 31, 124–130. URL: [http://linkinghub.elsevier.com/](http://linkinghub.elsevier.com/retrieve/pii/S1364815211002775)
690 [retrieve/pii/S1364815211002775](http://linkinghub.elsevier.com/retrieve/pii/S1364815211002775), doi:10.1016/j.envsoft.2011.11.014.

691 Ogino, S.Y., Yamanaka, M.D., Mori, S., Matsumoto, J., 2016. How Much is the Precipitation Amount
692 over the Tropical Coastal Region? *Journal of Climate* 29, 1231–1236. URL: [http://journals.](http://journals.ametsoc.org/doi/10.1175/JCLI-D-15-0484.1)
693 [ametsoc.org/doi/10.1175/JCLI-D-15-0484.1](http://journals.ametsoc.org/doi/10.1175/JCLI-D-15-0484.1), doi:10.1175/JCLI-D-15-0484.1.

694 Okeke, F., Karnieli, A., 2006. Methods for fuzzy classification and accuracy assessment of historical
695 aerial photographs for vegetation change analyses. Part I: Algorithm development. *International*
696 *Journal of Remote Sensing* 27, 153–176. URL: [https://www.tandfonline.com/doi/full/10.1080/](https://www.tandfonline.com/doi/full/10.1080/01431160500166540)
697 [01431160500166540](https://www.tandfonline.com/doi/full/10.1080/01431160500166540), doi:10.1080/01431160500166540.

698 Otieno, H., Yang, J., Liu, W., Han, D., 2014. Influence of Rain Gauge Density on Interpolation Method
699 Selection. *Journal of Hydrologic Engineering* 19, 04014024. URL: [http://ascelibrary.org/doi/10.](http://ascelibrary.org/doi/10.1061/%28ASCE%29HE.1943-5584.0000964)
700 [1061/%28ASCE%29HE.1943-5584.0000964](http://ascelibrary.org/doi/10.1061/%28ASCE%29HE.1943-5584.0000964), doi:10.1061/(ASCE)HE.1943-5584.0000964.

701 Paulat, M., Frei, C., Hagen, M., Wernli, H., 2008. A gridded dataset of hourly pre-
702 cipitation in Germany: Its construction, climatology and application. *metz* 17, 719–
703 732. URL: [http://www.schweizerbart.de/papers/metz/detail/17/56817/A_gridded_dataset_of_](http://www.schweizerbart.de/papers/metz/detail/17/56817/A_gridded_dataset_of_hourly_precipitation_in_Germa?af=crossref)
704 [hourly_precipitation_in_Germa?af=crossref](http://www.schweizerbart.de/papers/metz/detail/17/56817/A_gridded_dataset_of_hourly_precipitation_in_Germa?af=crossref), doi:10.1127/0941-2948/2008/0332.

705 Reid, I., 1973. THE INFLUENCE OF SLOPE ASPECT ON PRECIPITATION RECEIPT. *Weather*
706 28, 490–494. URL: [https://rmets.onlinelibrary.wiley.com/doi/abs/10.1002/j.1477-8696.1973.](https://rmets.onlinelibrary.wiley.com/doi/abs/10.1002/j.1477-8696.1973.tb00814.x)
707 [tb00814.x](https://rmets.onlinelibrary.wiley.com/doi/abs/10.1002/j.1477-8696.1973.tb00814.x), doi:10.1002/j.1477-8696.1973.tb00814.x.

708 Sanchez-Moreno, J.F., Mannaerts, C.M., Jetten, V., 2014. Influence of topography on rainfall variability
709 in Santiago Island, Cape Verde: INFLUENCE OF TOPOGRAPHY ON RAINFALL VARIABILITY
710 IN CAPE VERDE. *International Journal of Climatology* 34, 1081–1097. URL: [http://doi.wiley.](http://doi.wiley.com/10.1002/joc.3747)
711 [com/10.1002/joc.3747](http://doi.wiley.com/10.1002/joc.3747), doi:10.1002/joc.3747.

712 Sebastianelli, S., Russo, F., Napolitano, F., Baldini, L., 2013. On precipitation measurements col-
713 lected by a weather radar and a rain gauge network. *Natural Hazards and Earth System Sci-*
714 *ence* 13, 605–623. URL: <http://www.nat-hazards-earth-syst-sci.net/13/605/2013/>, doi:10.5194/
715 [nhess-13-605-2013](http://www.nat-hazards-earth-syst-sci.net/13/605/2013/).

716 Sevruk, B., Nevenic, M., 1998. The geography and topography effects on the areal pattern of precipitation
717 in a small prealpine basin. *Water Science & Technolog* 37, 163–170. doi:10.1016/S0273-1223(98)
718 [00329-1](https://doi.org/10.1016/S0273-1223(98)00329-1).

719 Sharon, D., Arazi, A., 1997. The distribution of wind-driven rainfall in a small valley: an empirical

720 basis for numerical model verification. *Journal of Hydrology* 201, 21–48. URL: <http://linkinghub.elsevier.com/retrieve/pii/S0022169497000346>, doi:10.1016/S0022-1694(97)00034-6.

721

722 Sideris, I.V., Gabella, M., Erdin, R., Germann, U., 2014. Real-time radar-rain-gauge merging using
723 spatio-temporal co-kriging with external drift in the alpine terrain of Switzerland: Real-time radar-
724 rain-gauge merging. *Quarterly Journal of the Royal Meteorological Society* 140, 1097–1111. URL:
725 <http://doi.wiley.com/10.1002/qj.2188>, doi:10.1002/qj.2188.

726 Sinclair, S., Pegram, G., 2005. Combining radar and rain gauge rainfall estimates using conditional
727 merging. *Atmospheric Science Letters* 6, 19–22. URL: <http://doi.wiley.com/10.1002/asl.85>,
728 doi:10.1002/asl.85.

729 Sternberg, M., Shoshany, M., 2001. Influence of slope aspect on Mediterranean woody formations:
730 Comparison of a semiarid and an arid site in Israel: Slope aspect differences in Mediterranean woody
731 formations. *Ecological Research* 16, 335–345. URL: <http://doi.wiley.com/10.1046/j.1440-1703.2001.00393.x>,
732 doi:10.1046/j.1440-1703.2001.00393.x.

733 Svoray, T., Mazor, S., Bar (Kutiel), P., 2007. How is Shrub Cover Related to Soil Moisture and Patch
734 Geometry in the Fragmented Landscape of the Northern Negev desert? *Landscape Ecol* 22, 105–116.
735 URL: <http://link.springer.com/10.1007/s10980-006-9004-3>, doi:10.1007/s10980-006-9004-3.

736 Svoray, T., Shafran-Nathan, R., Henkin, Z., Perevolotsky, A., 2008. Spatially and temporally explicit
737 modeling of conditions for primary production of annuals in dry environments. *Ecological Modelling*
738 218, 339–353. URL: <http://linkinghub.elsevier.com/retrieve/pii/S0304380008003827>, doi:10.
739 1016/j.ecolmodel.2008.07.029.

740 Tang, G., Long, D., Hong, Y., Gao, J., Wan, W., 2018. Documentation of multifactorial relationships
741 between precipitation and topography of the Tibetan Plateau using spaceborne precipitation radars.
742 *Remote Sensing of Environment* 208, 82–96. URL: <http://linkinghub.elsevier.com/retrieve/pii/S0034425718300130>,
743 doi:10.1016/j.rse.2018.02.007.

744 Todini, E., Alberoni, P., Butts, M., Collier, C., Khatibi, R., 2005. ACTIF best practice pa-
745 per–understanding and reducing uncertainty in flood forecasting, in: P. Balabanis, D. Lumbroso,
746 P. Samuels International conference on innovation, advances and implementation of flood forecast-
747 ing technology, Troms, Norway. URL: [http://www.academia.edu/download/38241880/ACTIF_best_](http://www.academia.edu/download/38241880/ACTIF_best_practice_paper_1_Uncertainty_in_flood_forecasting_V2.pdf)
748 [practice_paper_1_Uncertainty_in_flood_forecasting_V2.pdf](http://www.academia.edu/download/38241880/ACTIF_best_practice_paper_1_Uncertainty_in_flood_forecasting_V2.pdf).

749 Villarini, G., Krajewski, W.F., 2010. Review of the Different Sources of Uncertainty in Single Polarization
750 Radar-Based Estimates of Rainfall. *Surveys in Geophysics* 31, 107–129. URL: <http://link.springer.com/10.1007/s10712-009-9079-x>,
751 doi:10.1007/s10712-009-9079-x.

752 Villarini, G., Mandapaka, P.V., Krajewski, W.F., Moore, R.J., 2008. Rainfall and sampling uncertainties:
753 A rain gauge perspective. *Journal of Geophysical Research* 113. URL: <http://doi.wiley.com/10.1029/2007JD009214>,
754 doi:10.1029/2007JD009214.

755 Wang, X., Zheng, X., He, J., Li, X., 2012. Using fuzzy logic to discriminate convective and stratiform
756 precipitation in Doppler weather radar, in: 2012 9th International Conference on Fuzzy Systems and
757 Knowledge Discovery, pp. 623–627. doi:10.1109/FSKD.2012.6233819.

758 Wijitkosum, S., Sriburi, T., 2019. Fuzzy AHP Integrated with GIS Analyses for Drought Risk Assess-
759 ment: A Case Study from Upper Phetchaburi River Basin, Thailand , 16.

760 Yang, Y., Chen, X., Qi, Y., 2013. Classification of convective/stratiform echoes in radar reflectivity
761 observations using a fuzzy logic algorithm: PRECIPITATION CLASSIFICATION FROM RADAR.
762 *Journal of Geophysical Research: Atmospheres* 118, 1896–1905. URL: <http://doi.wiley.com/10.1002/jgrd.50214>,
763 doi:10.1002/jgrd.50214.

764 Zadeh, L.A., 1965. Fuzzy Sets. *Information and Control* 8, 338–353. URL: https://www.liphy.ujf-grenoble.fr/pagesperso/bahram/biblio/Zadeh_FuzzySetTheory_1965.pdf.

765

766 Zadeh, L.A., 1975. Fuzzy logic and approximate reasoning. D. eidel Publishing Company 30, 22.

767 Zadeh, L.A., 2008. Is there a need for fuzzy logic? *Information Sciences* 178, 2751–2779. URL: <http://linkinghub.elsevier.com/retrieve/pii/S0020025508000716>, doi:10.1016/j.ins.2008.02.012.

768

769 Zimmermann, H.J., 2013. Fuzzy Set Theory and Its Applications. Springer Netherlands, Dordrecht.

770 URL: <http://public.ebib.com/choice/publicfullrecord.aspx?p=3568591>. oCLC: 958538892.